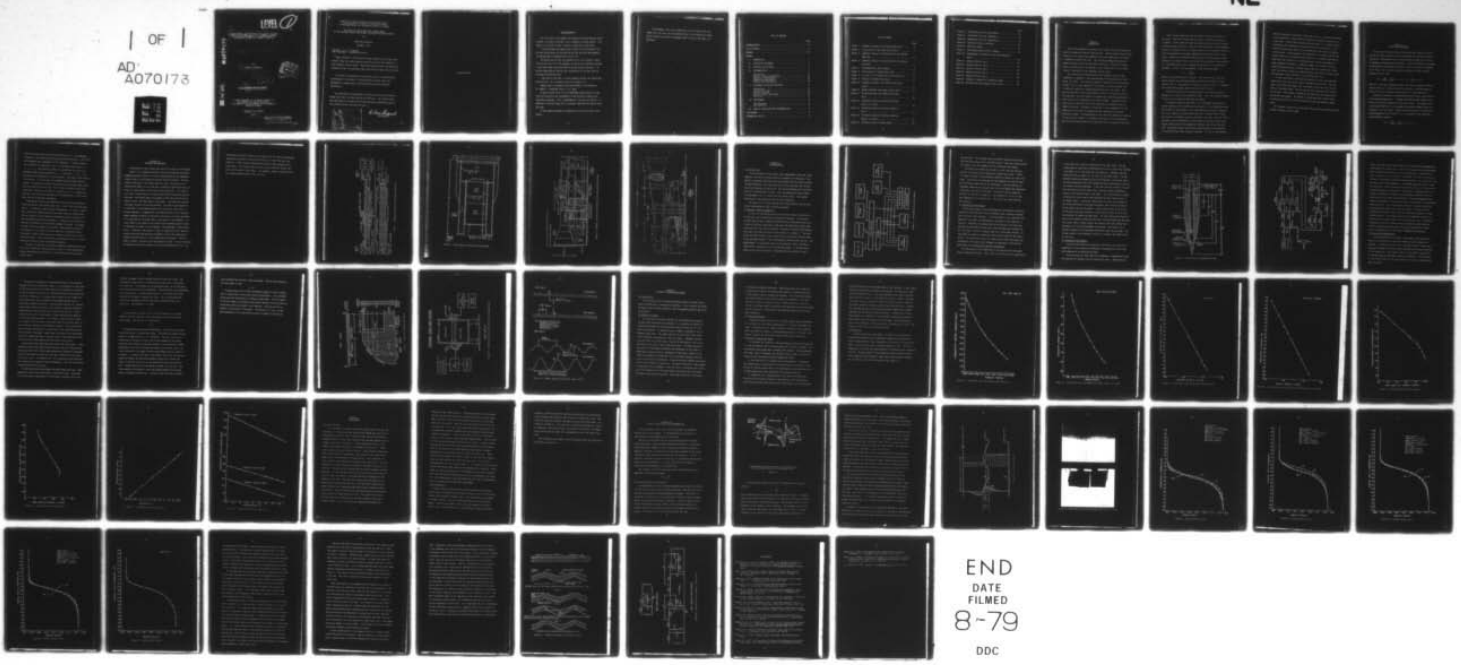
AD-A070 173 FLORIDA UNIV GAINESVILLE COASTAL AND OCEANOGRAPHIC --ETC F/G 20/4
AN EXPERIMENTAL INVESTIGATION OF THE EFFECT OF FINITE AMPLITUDE--ETC(U)
1975 T G TOMASELLO N00014-68-A-0173-0016
UNCLASSIFIED NL

| OF |
AD
A070173



END
DATE
FILMED
8-79
DDC

AD A070173

DDC FILE COPY

LEVEL I

(6) AN EXPERIMENTAL INVESTIGATION OF THE EFFECT OF FINITE AMPLITUDE INTERNAL WAVES AT THE INTERFACE BETWEEN TWO MISCIBLE FLUIDS ON THE DENSITY PROFILE

(9) Master's thesis,

BY

(10) THOMAS G. TOMASELLO

(11) 1975

(12) 63p.

(15) Contract N00014-68-A-0173-0016

DDC RECEIVED JUN 15 1979 C

A THESIS PRESENTED TO THE GRADUATE COUNCIL OF THE UNIVERSITY OF FLORIDA IN PARTIAL FULFILLMENT OF THE REQUIREMENTS FOR THE DEGREE OF MASTER OF SCIENCE

UNIVERSITY OF FLORIDA
Gainesville
1975
Coastal + Oceanographic Engr. Lab.

This document has been approved for public release and sale; its distribution is unlimited.

JOB

408 006 79 05 15 128

Abstract of Thesis Presented to the Graduate Council
of the University of Florida in Partial Fulfillment
of the Requirements for the Degree of Master of Science

THE EFFECT OF FINITE AMPLITUDE INTERNAL WAVES AT THE INTERFACE BETWEEN TWO MISCIBLE FLUIDS ON THE DENSITY PROFILE

by

Thomas Guy Tomasello

December, 1975

Chairman: Dr. D. M. Sheppard
Major Department: Engineering Sciences

Shear stresses in the interfacial layer created by finite amplitude internal waves can create unstable conditions and thus the formation of high frequency internal waves. These high frequency waves can enhance the diffusion of salt into the upper layer and affect the mass density profile.

The effect of these waves on the density profile is experimentally investigated in this thesis. Finite amplitude internal waves were generated for long periods of time and density profiles measured periodically.

The experiments were performed in an internal wave facility which is eighty feet long, four feet high and two feet wide. The internal waves were generated by a hydraulically driven horizontal diaphragm located at the interface and at one end of the tank.

D. Max Sheppard
Chairman

Accession For
NTIS GRA&I
DDC TAB
Unannounced
Justification
By
Distribution/
Availability Codes
Dist | Avail and/or special
A

79 05 14 128

to Jan and Tami

ACKNOWLEDGEMENTS

As I look back on the summer just passed and realize what was accomplished, it brings to mind how I am so indebted to so many people. This thesis, is the work of many, in which I played just a small part.

I wish to express my appreciation to many of the individuals that not only assisted me, but provided me with the necessary encouragement to continue when it appeared that all was lost.

The person most helpful and responsible for the successful completion of this work is Dr. Max Sheppard, my advisor and committee chairman. I have never known a more dedicated or harder working individual. It was his determination that was most responsible for the data that was wrestled from the wave tank.

I owe much to Ivan Chou, a fellow graduate student, who worked many hours with me. He is as much a part of the thesis as I.

Appreciation is extended to the other members of my committee, Dr. Robert L. Sierakowski and Dr. Yu H. Wang.

A special thanks to Dr. Harold Doddington whose expertise in the field of electronics was instrumental in the solution of many of our electronics problems. Also I acknowledge Mr. Jack Van Leer and Mr. J. D. McMillan for the work they did in the expert fabrication of much of what was used.

I thank Debbie Gatewood for preparation of the final copy of this thesis.

To my daughter, Tami, who I played very little kickball with this summer and to my wife, Jan, who helped so much in the reduction of data, who was patient and whose encouragement made it easier, this thesis is dedicated.

TABLE OF CONTENTS

	Page
ACKNOWLEDGEMENTS	iii
LIST OF FIGURES	vi
ABSTRACT	viii
CHAPTER	
I. INTRODUCTION	1
II. THEORETICAL BACKGROUND	4
III. APPARATUS AND EQUIPMENT	6
IV. INSTRUMENTATION	12
Introduction	12
Vertical Traversing Mechanism	12
Conductivity Measurements	14
Temperature Measurements	15
Internal Wave Measurements	18
V. INSTRUMENT CALIBRATION PROCEDURES	25
Introduction	25
Conductivity Probe	25
Position Indicator	26
Optical Internal Wave Gauge	26
Thermistor	27
VI. MEASUREMENTS	36
Test Procedure	36
Data Reduction	37
VII. RESULTS, CONCLUSIONS AND RECOMMENDATIONS	39
BIBLIOGRAPHY	55
BIOGRAPHICAL SKETCH	57

LIST OF FIGURES

		Page
Figure 1.	Schematic Drawing of the Internal Wave Tank	8
Figure 2.	Cross-section of Wave Tank Test Section	9
Figure 3.	Schematic Drawing of the North End of the Internal Wave Tank	10
Figure 4.	Schematic Drawing of the South End of the Internal Wave Tank	11
Figure 5.	Instrumentation, Block Diagram	13
Figure 6.	Cross-section of Conductivity Probe	16
Figure 7.	Circuit of the Conductivity Probe Electronics	17
Figure 8.	Drawing of Internal Wave Gauge	22
Figure 9.	Schematic Drawing of the Internal Wave Gauge System	23
Figure 10.	Graphic Recorder Chart Paper, Runs A and B	24
Figure 11.	Calibration Curve for Conductivity Probe, Run A	28
Figure 12.	Calibration Curve for Conductivity Probe, Runs B, C, D and E	29
Figure 13.	Calibration Curve for Position Indicator, Run A	30
Figure 14.	Calibration Curve for Position Indicator, Runs B, C, D and E	31
Figure 15.	Calibration Curve for Wave Gauge 4	32

Page

Figure 16. Calibration Curve for Wave Gauge 6 33

Figure 17. Calibration Curve for Thermistor 34

Figure 18. Temperature Effect on Conductivity 35

Figure 19. Velocity Profile at Interface 40

Figure 20. Definition Sketch 42

Figure 21. Anticipated Density Profile Changes 43

Figure 22. Photographs of Interfacial Layer and Interfacial Waves 44

Figure 23. Density Profiles, Run A 45

Figure 24. Density Profiles, Run B 46

Figure 25. Density Profiles, Run C 47

Figure 26. Density Profiles, Run D 48

Figure 27. Density Profiles, Run E 49

Figure 28. Schematic, Formation of Interfacial Waves 53

Figure 29. Pre-amplifier and Low-pass Filter Circuit 54

CHAPTER I
INTRODUCTION

Within the atmosphere and oceans of our planet exists the interesting physical phenomena of density stratification. Density stratification exists naturally in the oceans and atmosphere and is due primarily to variations in temperature within the fluid. The interfaces between these density stratified layers can be set into wave-like motion. These oscillations, known as internal waves, are thought by some researchers to be a primary source of turbulence in the atmosphere and the ocean.

The interaction of turbulence with electromagnetic waves in the atmosphere is important in the understanding of the propagation of these waves, Pao (1969). The energy dissipated in turbulence in the atmosphere on small scale is very important in the global scale energy budget, and is therefore important in global weather prediction, Pao (1969). Much work has been done in the investigation of clear air turbulence (CAT) in the atmosphere; and the breaking of internal waves has been suggested as a major cause of this turbulence, Hall and Pao (1969). Turbulence in the ocean plays an important role in the dispersion of pollutants that are added to the ocean. Turbulence in the ocean is also responsible for the dispersion of nutrients and oxygen which are important to the marine biological systems. An understanding of the turbulence generation mechanisms in the stratified oceans is of paramount importance to the oceanographer due to the overriding effects this turbulence has on the physical processes.

There is some controversy over the general nature of turbulence in the ocean. Long (1973) stated that the oceans are probably turbulent in general. Woods (1969) felt that the turbulence was confined to layers or patches within the fluid. Long (1973) discusses both of these theories. Mixing in a stagnant fluid or a laminar flow is due to molecular diffusion. The mixing processes are greatly enhanced by the introduction of turbulence. Transition to turbulent flow can result from the growth of a disturbance in an unstable flow. As with most flow situations, the stability of a stratified shear flow is governed by the value of a characteristic parameter. In this case the parameter is the Richardson number.

$$R_i = - \frac{g\rho'}{\rho(u')^2}$$

where g is the acceleration of gravity, ρ the mass density, u the horizontal velocity and the primes denote derivatives with respect to the vertical axis, z. Note that for a statically stable fluid ρ' is negative. The larger the Richardson number the more stable the flow.

The particle motion in an internal wave is such that the velocity gradient u' is large in the interfacial layer. Thus, the Richardson number is small in this region and the flow less stable.

The primary purpose of this work is to investigate the mixing processes induced by finite amplitude internal waves. Finite amplitude waves are defined for the purpose of this experiment as waves with a steepness ratio (a/λ, where a is the wave amplitude and λ the wave length) larger than that for infintesimal waves as defined by the linear stability theory. The waves in this experiment are linear waves as defined by linear wave theory, which requires the steepness of the wave ratio to be less than 0.04. Experiments where internal waves were generated at the interface in stratified fluids have long been conducted. As early as 1883 Osborne

Reynolds presented to the Royal Society the results of a study of the motion of two streams of a stratified fluid traveling in opposite directions in a closed tube. Thorpe (1967) generated internal waves in a closed horizontal rectangular tube containing a stratified fluid by raising one end. The resulting accelerating laminar flow provided sufficient shear to generate internal waves. The occurence of the instability, its nature, and the subsequent transition to turbulence were described. In another experiment by Wang (1972) the interface in a stratified shear flow was perturbed by a known frequency disturbance. Richardson numbers for unstable flow were determined experimentally and these values compared to theoretical values. Scotti and Corocos (1969) also conducted experiments wherein internal waves were generated at the interface of a stratified shear flow.

In this experimental investigation, interfacial waves were generated mechanically with a horizontal rubber diaphragm wave generator. Salt was used as the stratifying agent, with fresh water as the top layer and salt water as the bottom layer. Density profiles were obtained with a conductivity probe. Wave lengths, frequencies and amplitudes were measured with two optical wave gauges. The effects of finite amplitude internal waves on the density profile of the stratified fluid were experimentally determined.

For a general discussion of stratified flows and the associated stability problems involved, see Yih (1965).

CHAPTER II
THEORETICAL BACKGROUND

The study of the instability of stratified shear flows and the turbulence that often results is one of increasing practical and scientific importance. Rayleigh was the first to consider the stability of fluids of smoothly varying density distribution. Taylor and Goldstein considered two-dimensional disturbances in parallel flow of an inviscid, incompressible fluid. Their analysis leads to the governing linear stability equation for this flow.

$$\phi'' + \left[\frac{Ri}{(U-C)} - \frac{U''}{(U-C)} - \alpha^2 \right] \phi - \left[\phi' - \frac{U'}{U-C} \phi \right] K = 0$$

where Ri is the local Richardson number; the ratio of buoyancy forces to inertia forces, K is the variation of inertia due to the heterogeneity of the fluid, and ϕ' denotes the derivative of ϕ with respect to Z.

Boussinesq introduced an approximation which allows a simplification of the governing equations. In essence the approximation neglects the effect of the density gradient in the inertia terms. This appears to be a valid approximation for most geophysical problems; however, there are exceptions, see Long (1965). Neglecting the variation of inertia due to the heterogeneity of the fluid (i.e. K = 0) results in the simplified Taylor-Goldstein equation

$$\phi'' + \left[\frac{Ri}{(u-c)^2} - \frac{u''}{(u-c)} - \alpha^2 \right] \phi = 0$$

where the primes denote derivatives with respect to z. The dependent variable ϕ is the amplitude function of the stream function $\psi = \phi e^{i\alpha(x-ct)}$ and represents the z dependence of the disturbance. The wave number of the disturbance is denoted by α and c is the complex wave speed, i.e. $c = c_r + i\, c_i$. The imaginary portion of c determines the rate of disturbance growth or decay (growth for $c_i > 0$, decay for $c_i < 0$). c_r is the velocity of propagation of the disturbance. The primary flow velocity is given by U. Ri is the local or gradient Richardson number defined earlier. As pointed out earlier the value of the Richardson number determines the stability of this flow. Miles (1961) and Howard (1961) have shown that a sufficient condition for stability is $Ri > \frac{1}{4}$, everywhere in the flow. This result was obtained for an incompressible, inviscid flow model with an infintesimal disturbance.

Experiments to verify this theoretical work have been performed by Scotti and Corcos (1971) and by Wang (1972). Their results indicate that the $Ri > \frac{1}{4}$ criterion is good for small disturbances. In Scotti's experiment a statically stable stratified free shear layer was formed within the test section of a wind tunnel by merging two uniform streams of air after uniformly heating the top section. A vibrating wire was used to generate a disturbance at the interface between the layers. The growth or decay of this disturbance was observed. Wang generated interfacial disturbances in a two-layer stratified flow with a vibrating ribbon. The growth or decay of these waves was recorded along with the overall Richardson number. Wang's results were in agreement with Hazel's (1972) numerical solution of the Taylor-Goldstein equation.

This work, in addition to providing information regarding the mixing due to finite amplitude internal waves, is part of a more comprehensive program investigating the stability of finite amplitude internal waves in shear flows.

CHAPTER III
APPARATUS AND EQUIPMENT

A description of the internal wave facility is given in this Chapter.

Figure 1 is a schematic drawing of the facility showing the overall dimensions and the location of various testing apparatus and components. Figure 2 shows a cross-section of the wave tank test section. The test section of the tank is 24.4 meters (80 ft.) long, 1.22 meters (4 ft.) high and 0.61 meters (2 ft.) wide and is enclosed on both sides with 1.27 cm (½ in.) glass panels to facilitate visual observation. Two 16,960 ℓ (4,111 gal.) storage tanks are situated outside the building housing the wave tank. The storage tanks are elevated so that the wave tank may be gravity filled. One tank contains fresh water. The other tank contains salt water colored with red food coloring. The internal wave generator is contained in the enlarged section at the north end, (see Figure 3). The wave generator is comprised of a horizontal 0.96 m X 0.96 m neoprene rubber diaphragn attached to the walls of the tank at its outer perimeter. It is activated by a vertical shaft at the center of the diaphragm. Circular plates at the center of the internal wave diaphragm provide a means of connecting the shaft to the diaphragm. The diaphragm is hydraulically driven. A hydraulic power supply is used in conjunction with a hydraulic actuator and associated electronic equipment to drive the diaphragms to produce sinusoidal waves of varying amplitude and frequency. The piers shown in Figure 3 are part of the wave generator system. They are necessary to prevent mixing at the interface resulting from diaphragm action. The

wave energy dissipators located at the south end of the tank are galvanized expanded metal baskets filled with stainless steel lathe shavings, (see Figure 4). These units are positioned to dissipate both surface and internal waves. The internal wave facility is quite versatile and has features not discussed in this thesis. See Sheppard, Shemdin, and Wang (1973) for a complete description of this facility.

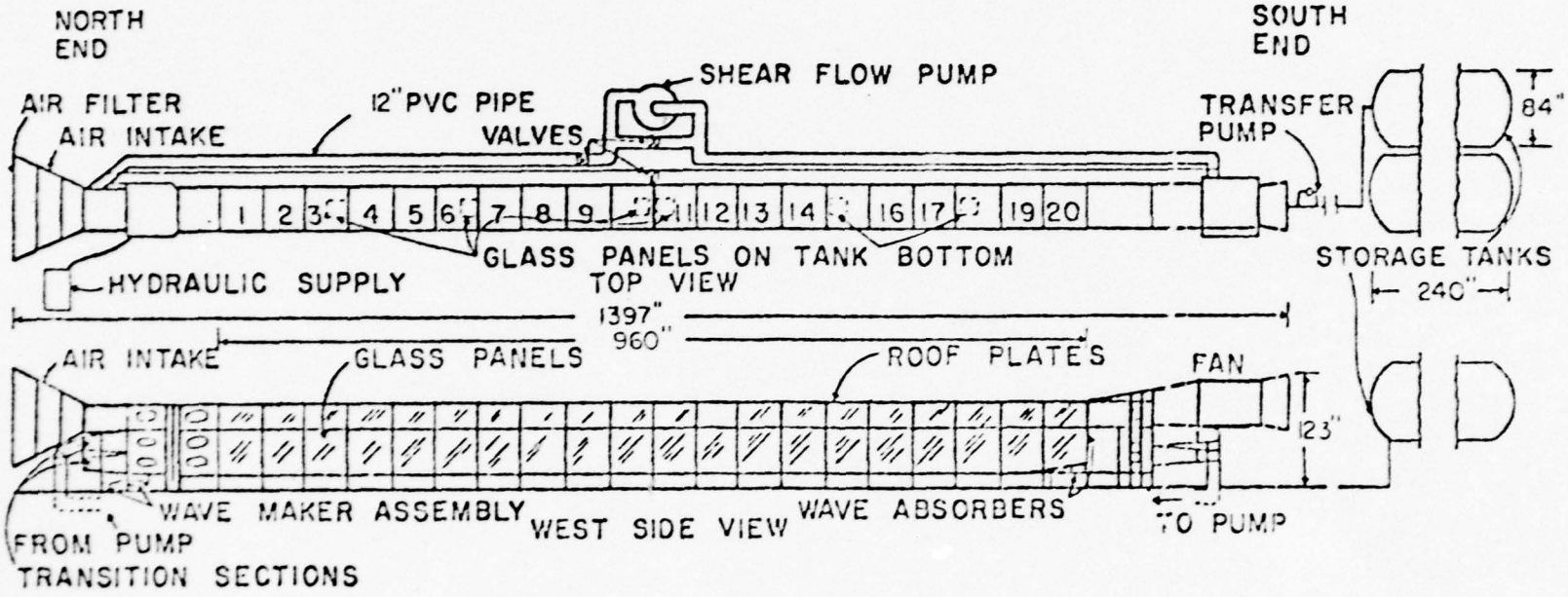


Figure 1. Schematic Drawing of the Internal Wave Tank

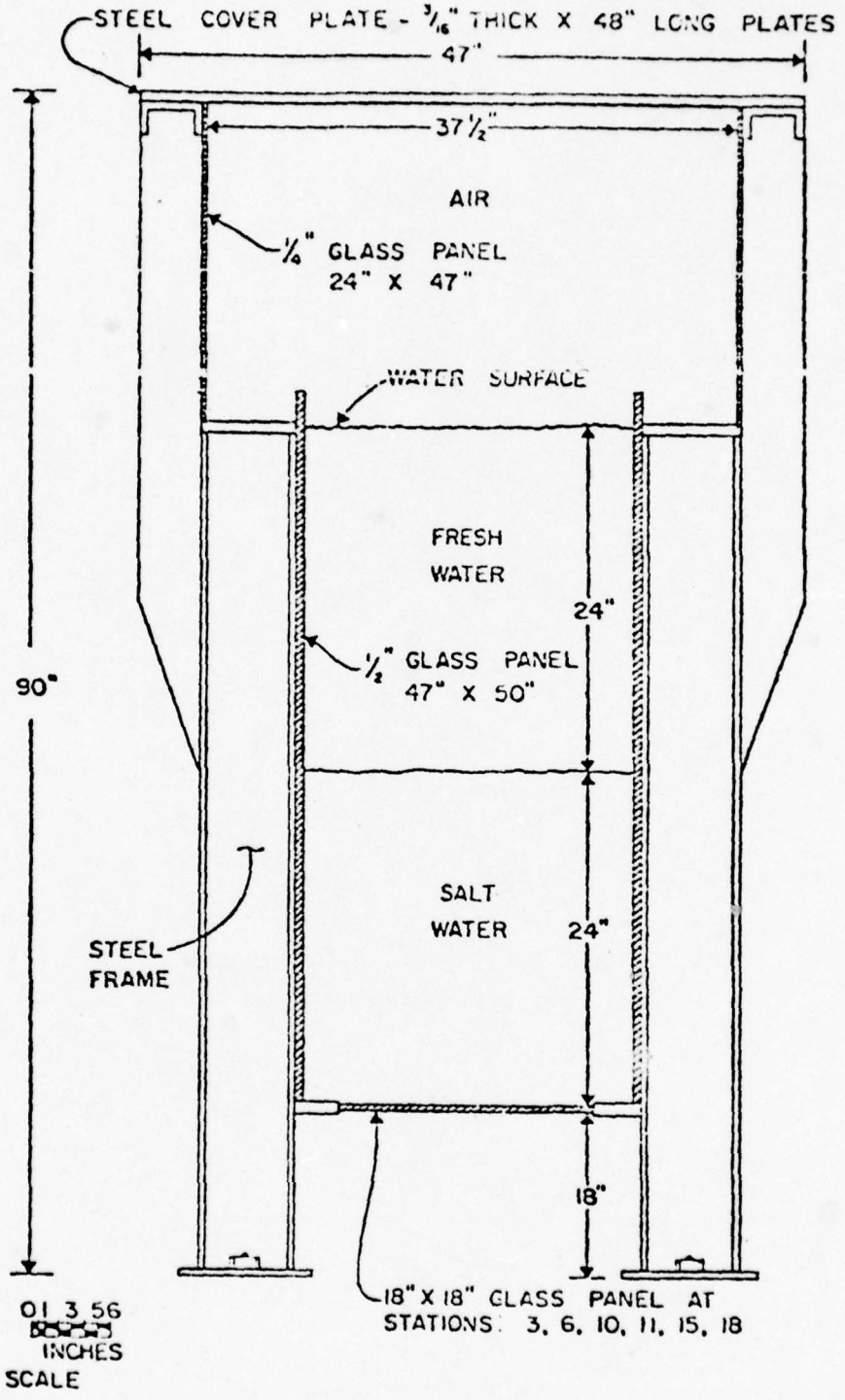


Figure 2. Cross-section of Wave Tank Test Section

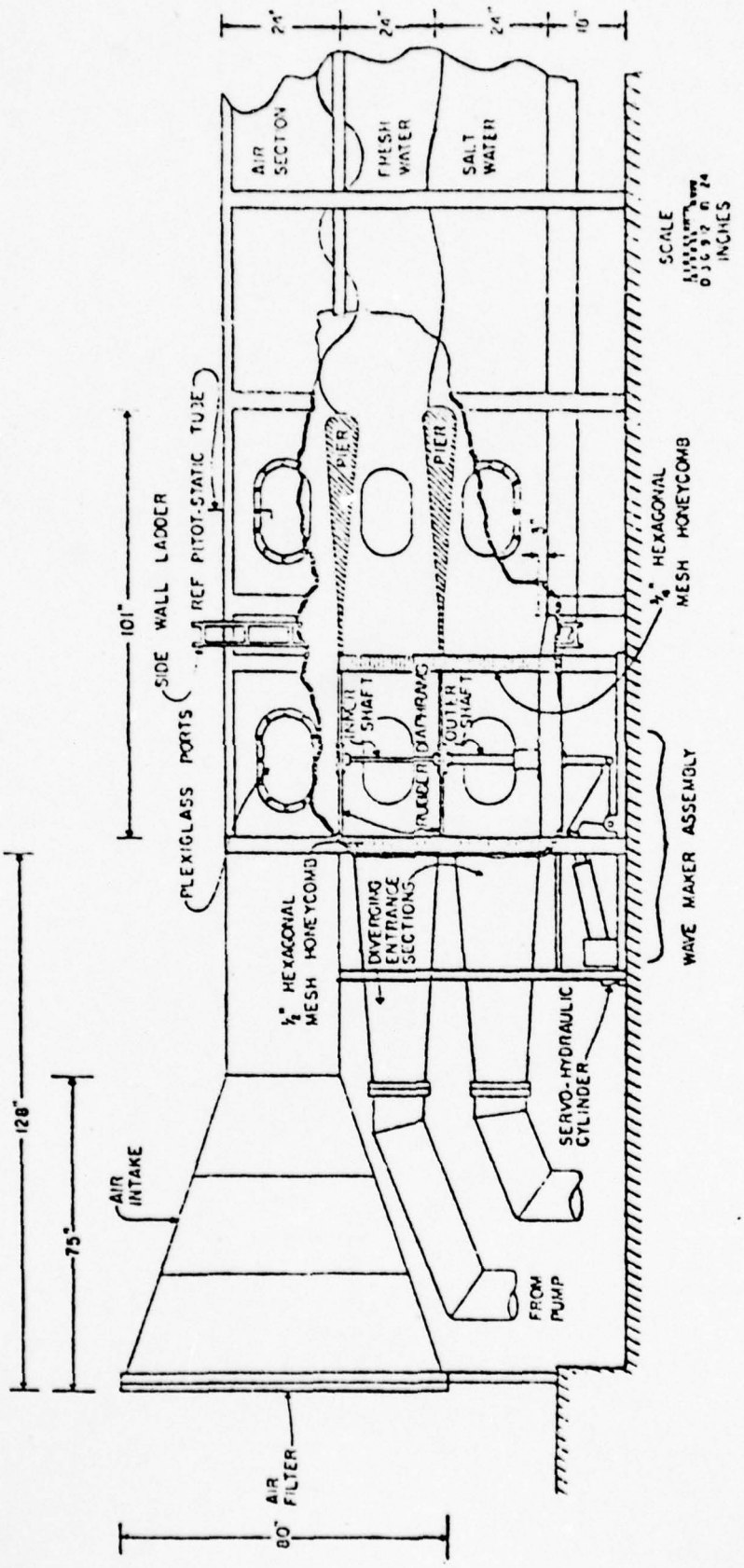


Figure 3. Schematic Drawing of the North End of the Internal Wave Tank

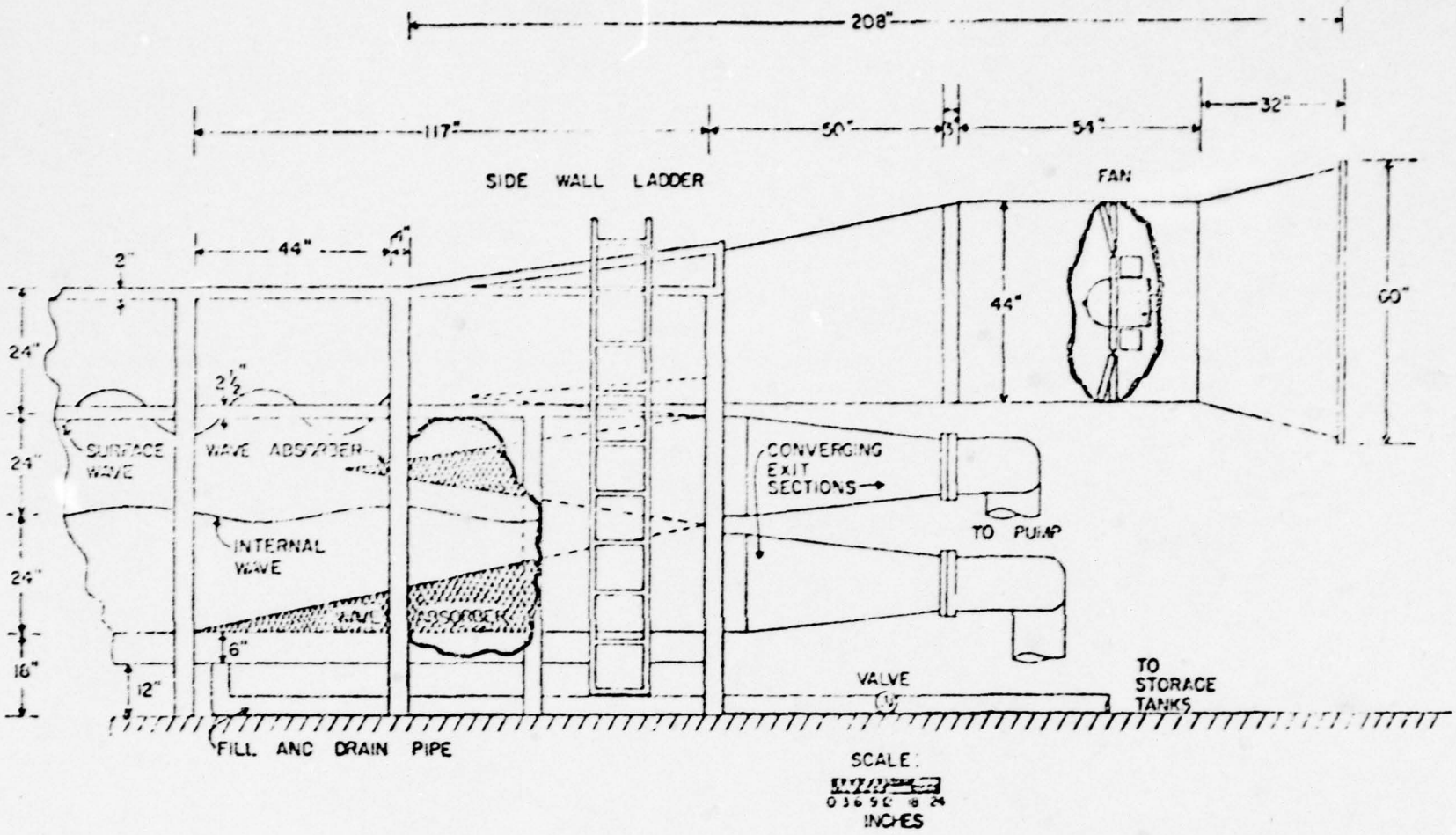


Figure 4. Schematic Drawing of the South End of the Internal Wave Tank

CHAPTER IV
INSTRUMENTATION

4.1 Introduction

In an experiment of this nature, point measurements requiring a high degree of resolution of certain physical parameters are necessary. Commercial instruments that meet these requirements were not always available. The great majority of the instrumentation used at the wave tank facility was custom designed and fabricated. Many design problems were associated with the instrumentation involved. Each item progressed through stages of development, until it reached the functioning stage. This chapter describes the instrumentation used in these experiments.

See Figure 5 for a block diagram of the instrumentation and the electrical interconnections used in these experiments.

4.2 Vertical Traversing Mechanism

In order for the sensing devices to accurately reach a desired point in the flow, special positioning equipment was designed. A reversible variable speed DC motor remotely controlled from the equipment room drives a vertical stainless steel shaft, upon which the conductivity probe, thermistor and hot film probe are mounted. The shaft is located midway between the sides of the tank at station 7 (see station 7 in Figure 1). The motor drives the shaft through a gear reduction box to reduce the traverse speed. A ten-turn potentiometer is also simultaneously driven by the gear box. The potentiometer, in conjunction with a series resistor, forms a voltage divider which is connected to a 15 volt DC power supply. A voltage proportional to the vertical position is obtained from the junction of these

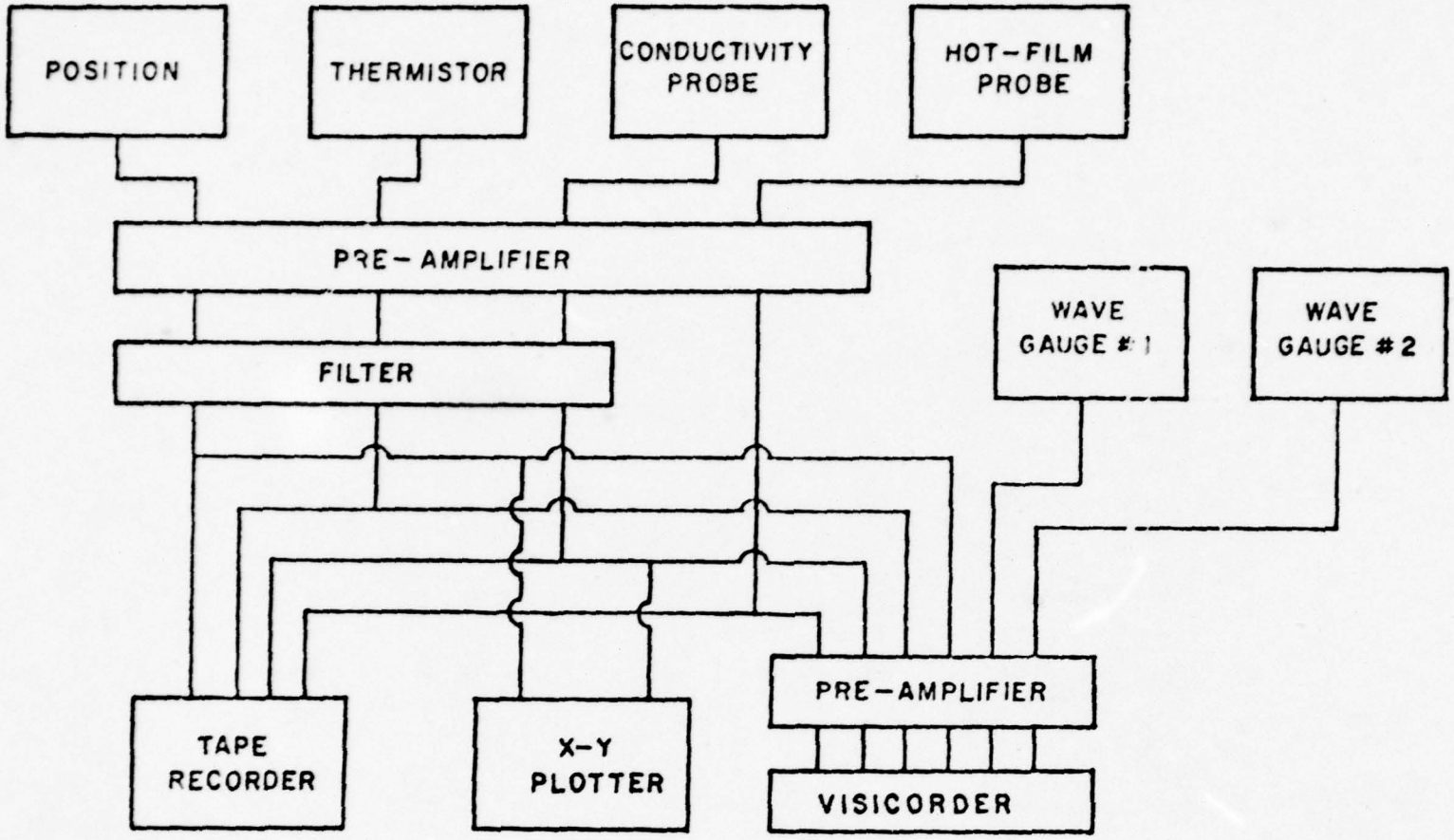


Figure 5. Instrumentation, Block Diagram

two resistors. This voltage, when calibrated, indicated the vertical position of the probe and is recorded on both a chart and a tape recorder. See Figure 12 for the schematic of this voltage divider network.

The probes are mounted on the shaft in such a way that they are parallel to the passing two-dimensional internal wave crest. Profile "E" shown in Figure 27 was acquired by making a traverse at a very slow speed. The profile thus obtained was then compared to a profile taken at the traverse speed used in the experiments. The two profiles corresponded; therefore the response time of the instruments was considered sufficient to be used at this speed. This can be seen by comparing profiles "E" and "D2" in Figure 26. The traverse for profile "E" was made immediately after profile "D2". As can be seen, these profiles are identical.

4.3 Conductivity Measurements

The primary purpose of this experiment was to determine the density profiles of the stratified fluid at different times following different wave activity at the interface. For the purposes of this experiment the density of each layer was determined by the amount of NaCl that was in solution. Therefore, the conductivity of the solution is directly proportional to the density of the fluid since the electrical conductivity of a salt water solution is greater than for a fresh water solution. An instrument was designed, fabricated, modified and tested for this application. The conductivity measuring system used in these experiments was developed for this work by Drs. Sheppard and Doddington (submitted for publication in the Review of Scientific Instruments).

For the purpose of this experiment it was necessary that the probe have two important features. First, that it could measure the conductivity

at any level with a vertical resolution of less than 0.5mm. This was accomplished by selectively withdrawing the fluid at a given level through a horizontal slot in the probe tip (see Figure 6). Secondly, that the probe would not be subject to a DC drift in the output signal. Earlier designed probes were plagued by such drift problems in the output signal. The probes plagued by this drift problem had gross differences in the surface area of the two electrodes. It was felt that this resulted in a partial rectification of the input signal, causing a higher resistance to current in one direction than in the other. This rectification can cause a migration of ions to one of the electrodes and thus cause a drift in the output signal. The partial rectification can also cause changes in the surface chemistry of the probe electrodes, which alters the rectification process and thus the output. Output signal drifts of up to 20% of the output value were noticed in time periods as small as 10% of the time required to conduct the experiment. The drift problem has been minimized in this probe by using two relatively large electrodes and confining the current flow to a small area of the vertical hole that connects the horizontal slit to the innerchamber of the probe. See Figure 7 for a schematic diagram of the associated electronics used with the probe. The voltage output of the electronics circuit is related to the conductivity of the fluid.

4.4 Temperature Measurements

Since both mass density and electrical resistivity are functions of temperature, it was necessary to determine the temperature of the fluid being measured by the conductivity probe.

The resistivity of a NaCl solution is dependent on temperature as are the conductivity readings from the conductivity probe. Temperature gra-

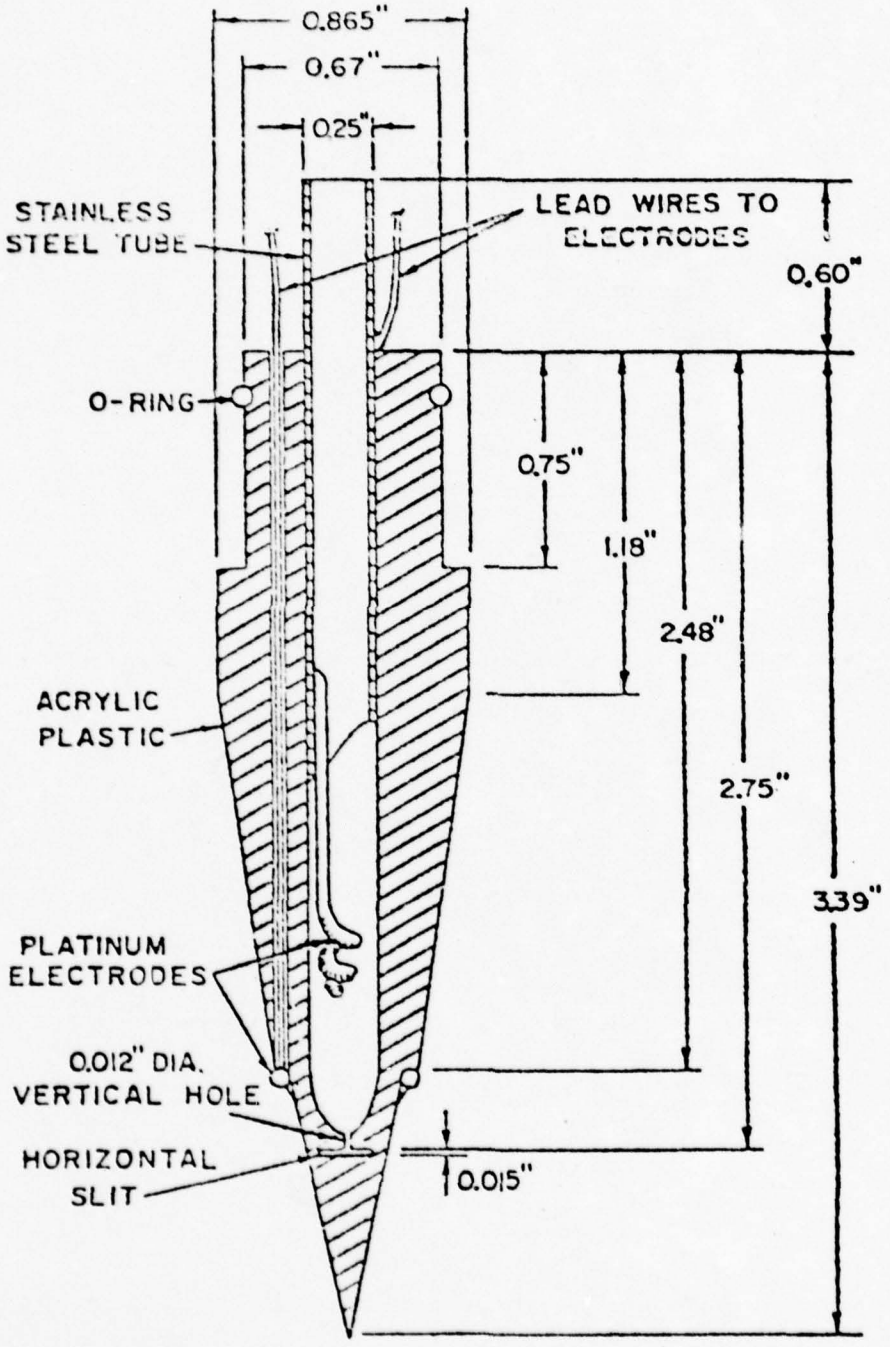


Figure 6. Cross-section of Conductivity Probe

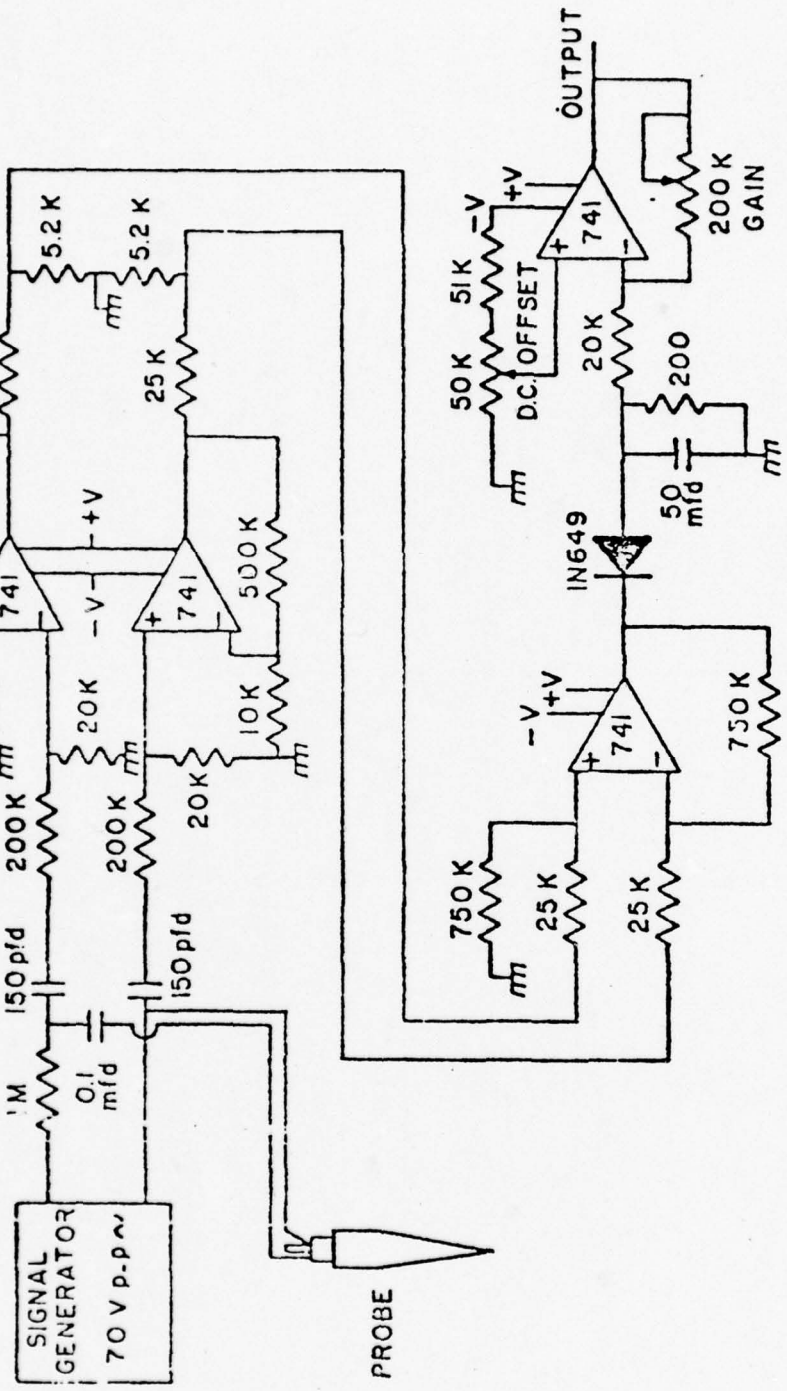


Figure 7. Circuit of the Conductivity Probe Electronics

dients also affect the stratification of the fluid under consideration by the formation of thermoclines. Since it is necessary to make measurements while the testing instruments are in vertical motion, a device with as small a response time as possible is desirable. For this reason and for reasons of convenience a thermistor bead was chosen. The resistance of the thermistor varies with temperature. A DC power supply was used to power the thermistor. Other resistors are used in the circuit to linearize the resistance change with temperature. Variations in temperature result in changes in thermistor resistance and subsequently variation of the voltage output of the voltage divider network. Since the temperature differences encountered in this work were small, the changes in the thermistor output were small. This necessitated the use of a high-gain amplifier with adjustable DC offset to process the signal. The amplifier also isolated the thermistor signal, with its low output impedance, from the recording device. The voltage output from the thermistor amplifier is linear as can be seen in Figure 17, the calibration curve. The effects of temperature were not known but were experimentally determined and found to be negligible (see Figure 18 for the relationship of conductivity to temperature) for the range of temperature encountered.

4.5 Internal Wave Measurements

In this experiment the frequency, wave length, celerity and wave height of the mechanically generated interfacial waves needed to be measured. To enable this to be done a laboratory optical internal wave gauge was designed, fabricated, tested and modified for proper operation in this application. See Figures 8 and 9 for the physical description of the wave gauge and necessary electrical connections. The following is a brief description of the gauge and how it is used to determine the above quantities.

The object of the gauge is to monitor the motion of the interface between the salt and fresh water layers. It is necessary that one layer of the fluid be dyed and the other layer be as transparent as possible. The system consists primarily of a custom-built optical light sensor and a parallel light source. The power supply voltage for the lights must be regulated since small variations in this supply voltage result in large light intensity variations. The wave gauge consists of a cadmium sulfide photo sensitive resistor, and a parabolic reflector designed to concentrate the light received by the gauge on the resistor. As the interface rises or falls the amount of light received by the photo resistor varies proportionately. This change in light intensity results in a change in the resistance in the photo sentitive resistor, which in turn causes an unbalance of the Wheatstone bridge. This unbalance produces an output voltage that is proportional to the interface position. The mid point of the gauges' linear range is located at the undisturbed interface. Red dye was used in the salt layer to take advantage of the low sensitivity of the cadmium sulfide resistor to red light.

Originally 50 watt spotlights were used as the light sources. These spotlights proved undesirable because the point source of light did not produce parallel light. After some problems with linearity of the gauge output it was determined that the light source should be a line source of parallel light. To accomplish this, 18" fluorescent lights were used with reflectors and honeycomb light straighteners. This new light source accomplished the desired results.

To make the required measurements two wave gauges were used. These gauges were located 2.44 meters apart at stations 4 and 6. The output of the wave gauge bridge network is fed through a pre-amp circuit that

isolates the gauge from the recorder and also filters the signal. The wave gauge voltage output is recorded on chart paper and is referenced to a time grid. The frequency of the interfacial waves can be calculated once the wave period has been determined. The wave period can be determined by the wave gauges. To measure wave period, T, is to measure the time required for the wave to complete one cycle. This is obtained by measuring the time between crests on the graphic recording output (see Figure 10). The frequency, f, is then

$$f = \frac{1}{T}$$

For the waves in question, their ratio of amplitude, a, to wavelength L, was such that they can be considered to be finite amplitude linear waves. The celerity (c) is defined by

$$c = \frac{L}{T}$$

The wave period was previously determined. The celerity can be measured with the use of the two wave gauges. The distances between the wave gauges is a known quantity; i.e., 2.44 meters. The time required for a given point on the wave to travel the distance between the two gauges divided by this distance is the wave celerity. For convenience in these experiments, the crest of the wave was used as the reference point. By visual observation, the number of wave crests between the wave gauges is estimated. In viewing the output of the graphic records for the two wave gauges and knowing the approximate number of wave crests between the gauges, a specific wave crest can be identified on both wave gauge outputs. The horizontal axis of the graphic recorder is a time axis. The time required for the wave to travel the distance between the two wave gauges is measured from this axis. With this time to distance relation-

ship available the celerity is then calculated. From the above equation, the wave length is then

$$L = cT$$

The wave gauges used in these experiments produce an output voltage that is proportional to the actual physical wave height. The calibration curves give the relationship of voltage to wave height. From the output of the wave gauges as recorded on the graphic recorder and the calibration curves the actual wave heights can be measured. See Figure 10 for an example of the outputs of the gauges. The values of f, c and L of the waves generated in this experiment are given in Figures 23 through 26.

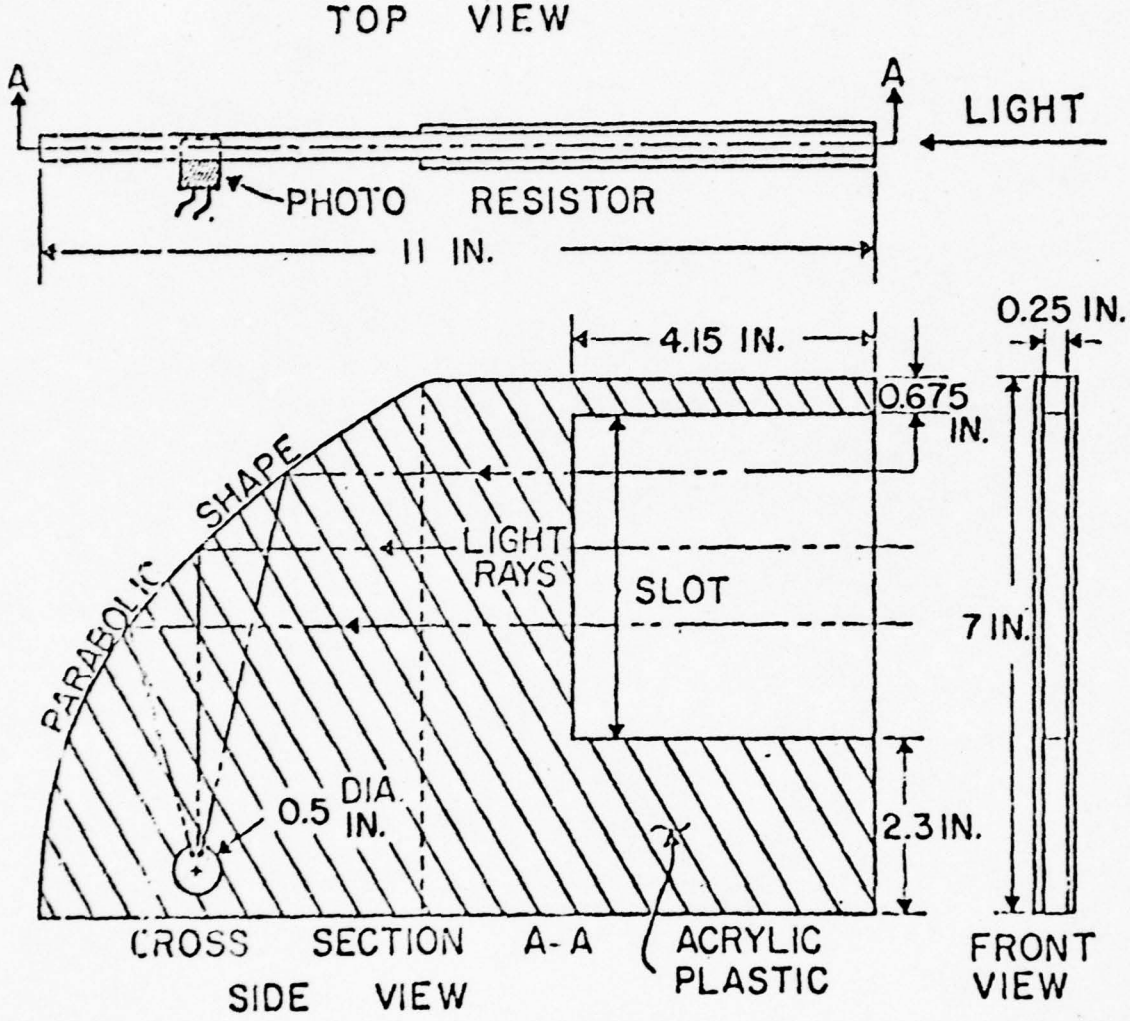


Figure 8. Drawing of Internal Wave Gauge

INTERNAL WAVE GAGE SYSTEM

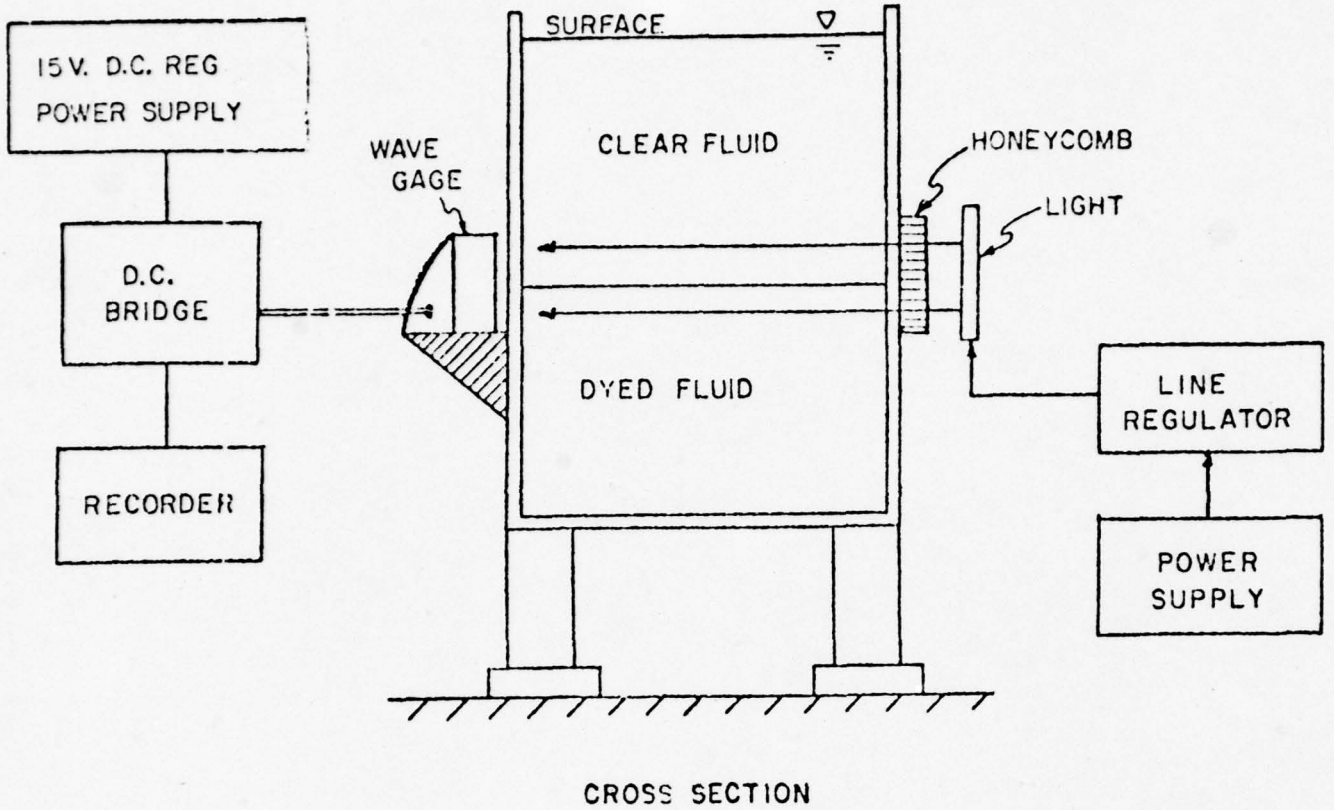
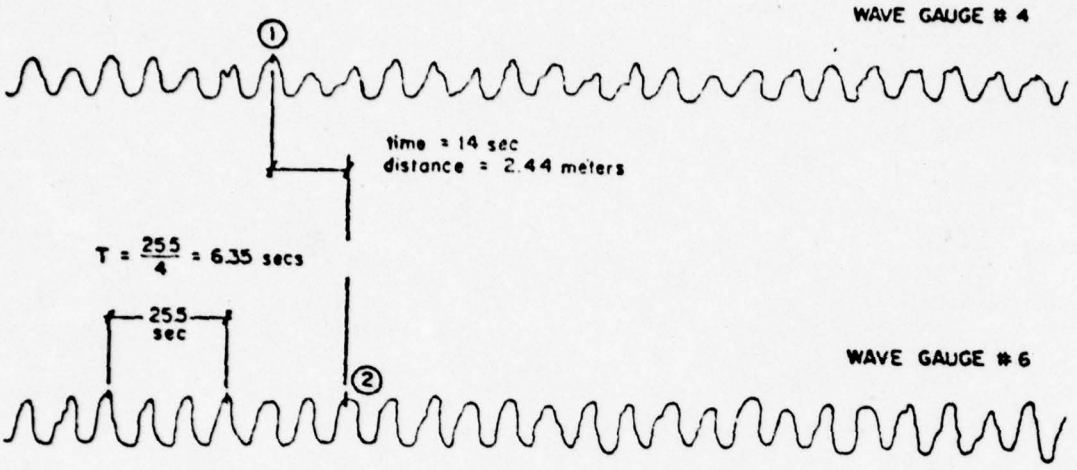


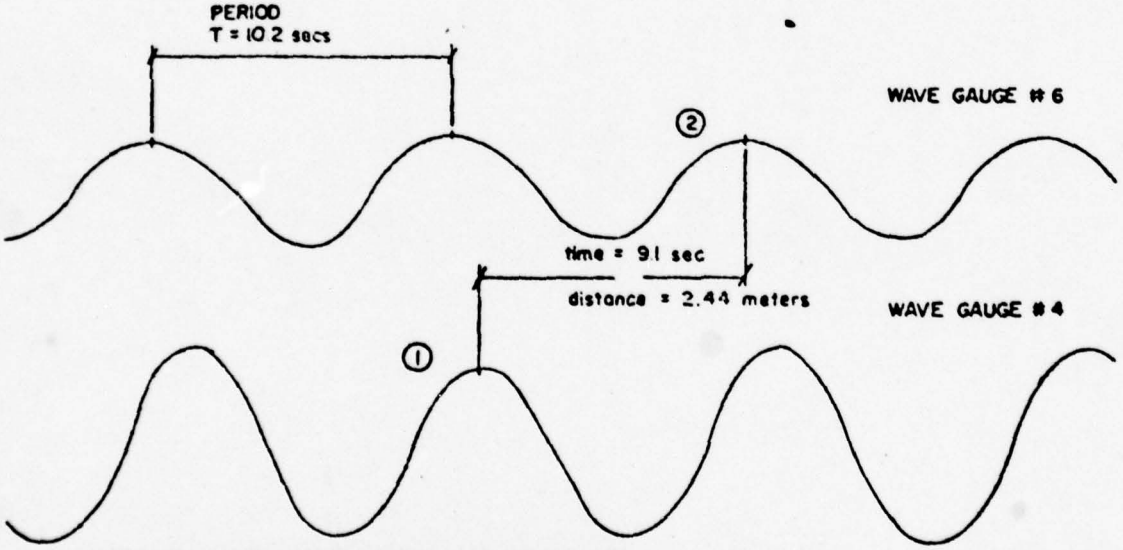
Figure 9. Schematic Drawing of the Internal Wave Gauge System

TEST RUN 'A'



NOTE: BY VISUAL OBSERVATION IT IS ESTIMATED THAT THERE ARE 2 WAVES BETWEEN WAVE GAUGES # 4 & # 6. THE GAUGES ARE 96" APART. SEE CREST LABELED ① & ②

TEST RUN 'B'



NOTE: BY VISUAL OBSERVATION IT IS ESTIMATED THAT THERE IS ONE WAVE BETWEEN GAUGES 4 & 6. SEE CREST LABELED ① & ②

Figure 10. Graphic Recorder Chart Paper, Runs A and B

CHAPTER V
INSTRUMENT CALIBRATION PROCEDURES

5.1 Introduction

The transducers used in these experiments produce an output voltage that is proportional to some physical quantity. In this chapter the method of relating these voltage readouts to the corresponding physical quantities is discussed.

5.2 Conductivity Probe

In order that the voltage readings from the conductivity probe and its associated electronics be meaningful, it is necessary to establish a relationship between the voltage and the specific gravity of the fluid under investigation. To accomplish this a siphon is attached to the instrument probe shaft. The siphon consists of a disc and a cone, 0.800 inch in diameter, separated by a 0.015 inch space. Attached to the disc is a 3/16 inch I.D. plastic tube. The slot of the siphon is set to the same level as the slot in the conductivity probe. The bottom portion of the siphon is cone shaped to minimize the disturbance as the siphon is moved down through the fluid. Beginning in fresh water, samples of the fluid are siphoned off through the slot at different positions along the z axis and collected in containers. Conductivity probe readings were taken prior to the siphoning at each level. The specific gravity of these samples is determined with a hydrometer. Since the fluid is stratified and at rest, the fluid siphoned off has the same specific gravity as the fluid being analyzed by the conductivity probe. (See Turner (1973) for a discussion

of selective withdrawal processes). Moving the probes until there was a significant change in the conductivity voltage, a reasonable spacing in the specific gravity readings was obtained. The relationship between the voltage readout and the specific gravity was obtained. This relationship is shown in Figures 11 and 12. These calibration curves are linear at the lower specific gravities and slightly nonlinear at the higher specific gravities. Calibration of the probe was done before and after each experiment.

5.3 Position Indicator

Since the position indicator is a voltage divider network consisting of a resistor and a multiturn potentiometer, it is linear throughout its range. Calibration then is simply a matter of relating voltage readings out of the resistive network to corresponding positions in the tank. See Figures 13 and 14 for calibration curves of the position indicator.

5.4 Optical Internal Wave Gauge

To determine the linearity of the wave gauges, an opaque card was used to cover the opening slot of the wave gauges at 1/10 inch increments. The corresponding wave gauge output voltages were recorded. After determining the linear range of the gauge, the mid point of this range on the slot is located at the undisturbed interface between the fluids.

As described earlier in Chapter IV on instrumentation, the optical wave gauge output is proportional to the position of the interface. Calibration of the wave gauges consists of experimentally determining the relationship between the output voltage and the interface position.

To accomplish this, attempts were at first made to determine the location of the interface adjacent to the gauge by visual observations. Determining accurately the location of the interface by visual observation

was difficult due to the diffused nature of the interface. A very simple method to overcome this problem was discovered. The fresh water layer was not completely filled. This made available an air-water interface which was easily read to a high degree of accuracy. While filling the salt water layer, a variation of position of this air-water interface accurately reflects a position change of the fresh-salt water interface. All that remained was to determine the distance between the air-water interface and the fresh-salt water interface. A small error in this determination is acceptable if the amplitude of the generated waves remains within the linear range of the wave gauge. This procedure was used in the calibration of the wave gauges at station Nos. 4 and 6. See Figures 15 and 16 for the calibration curves.

5.5 Thermistor

As with the previous instruments, calibration of the thermistor, consisted of determining the relationship between the thermistor electronics output and the actual temperature of the fluid at the thermistor bead. This was done by using a constant temperature bath. The fluid temperature in the bath was determined with a thermometer with graduations of $0.2^{o}F$. Voltage readouts of the thermistor high-gain amplifier and fluid temperature were recorded. These values when plotted resulted in the calibration curve for the thermistor (see Figure 17).

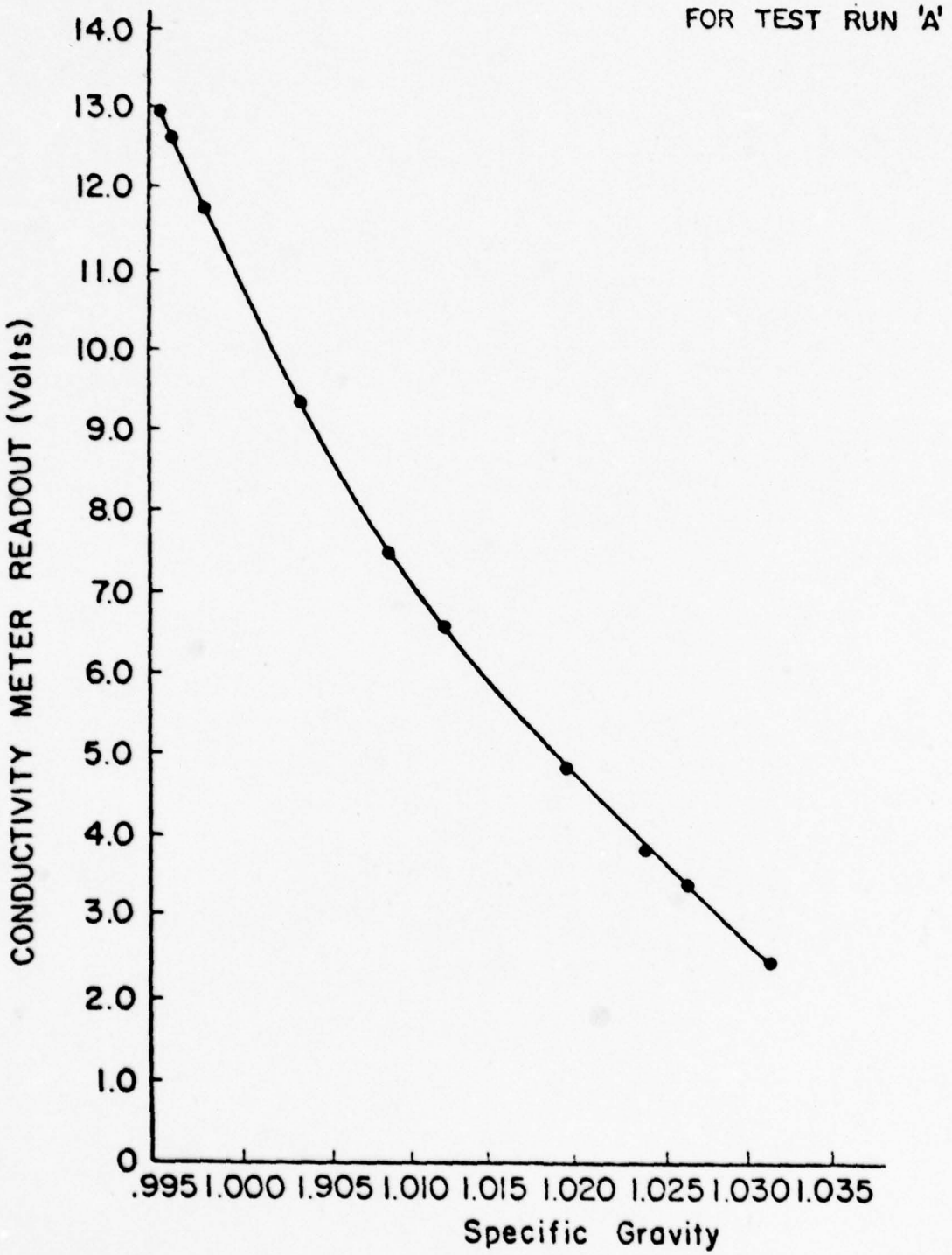


Figure 11. Calibration Curve for Conductivity Probe, Run A

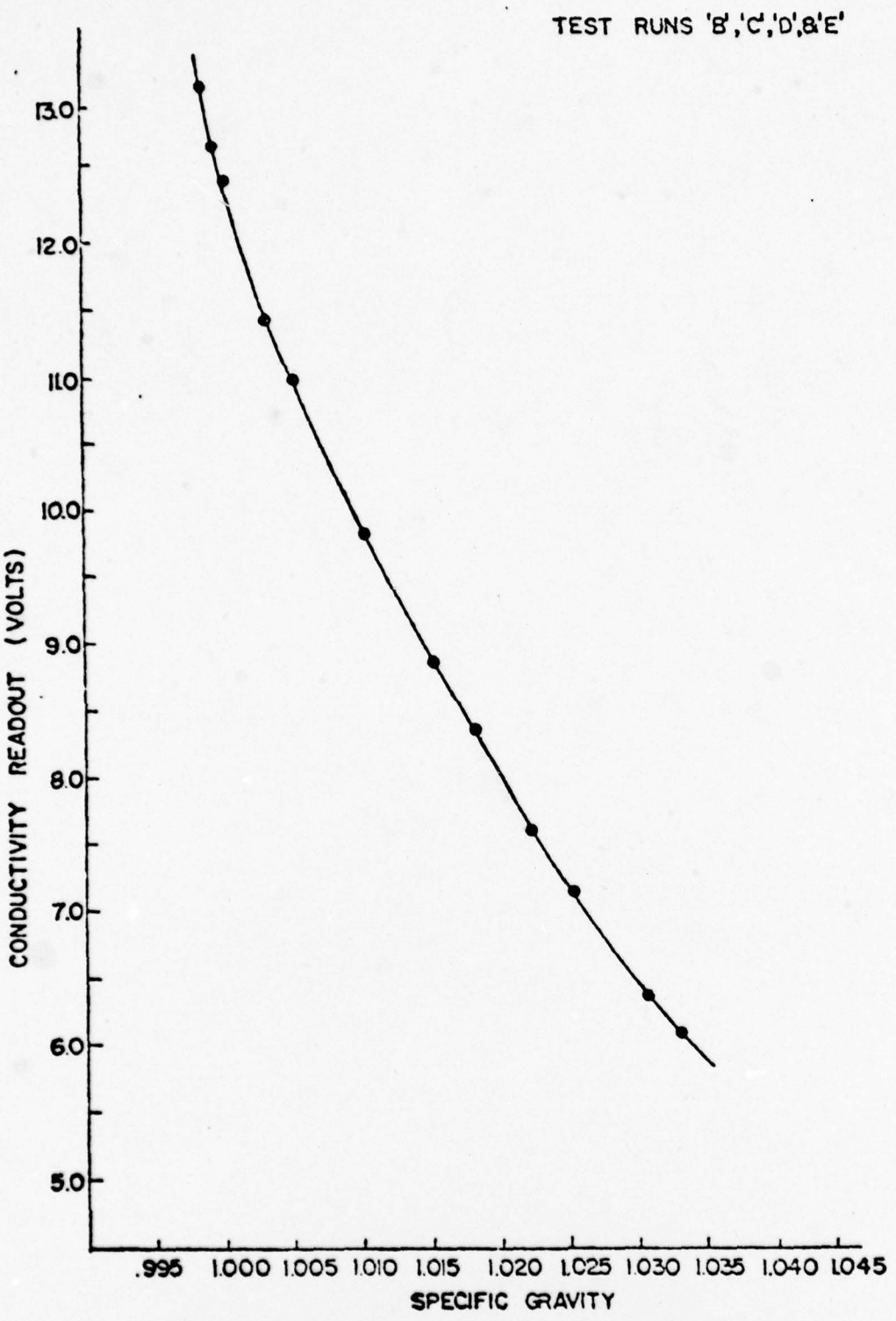


Figure 12. Calibration Curve for Conductivity Probe, Runs B, C, D and E

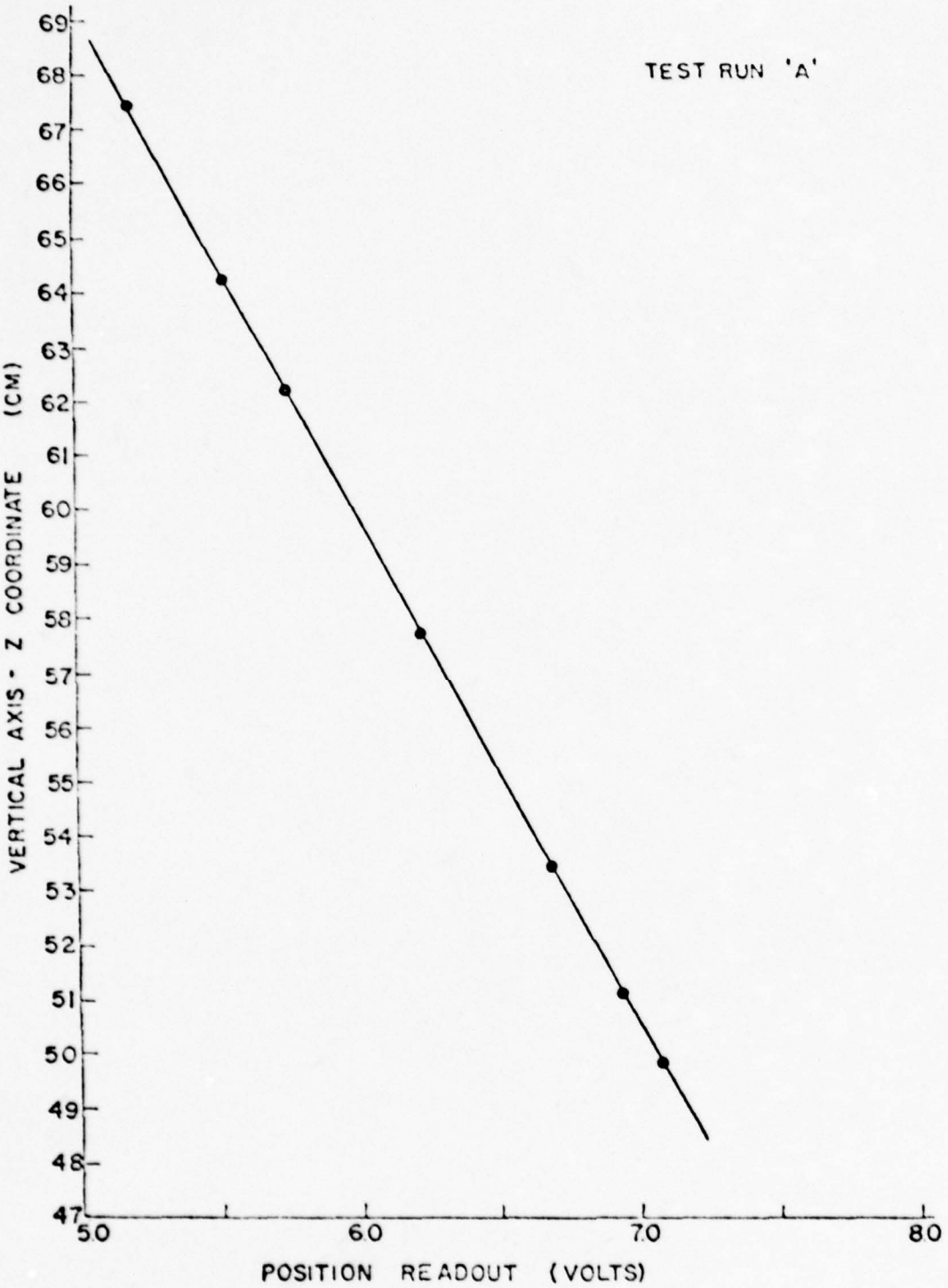


Figure 13. Calibration Curve for Position Indicator Run A

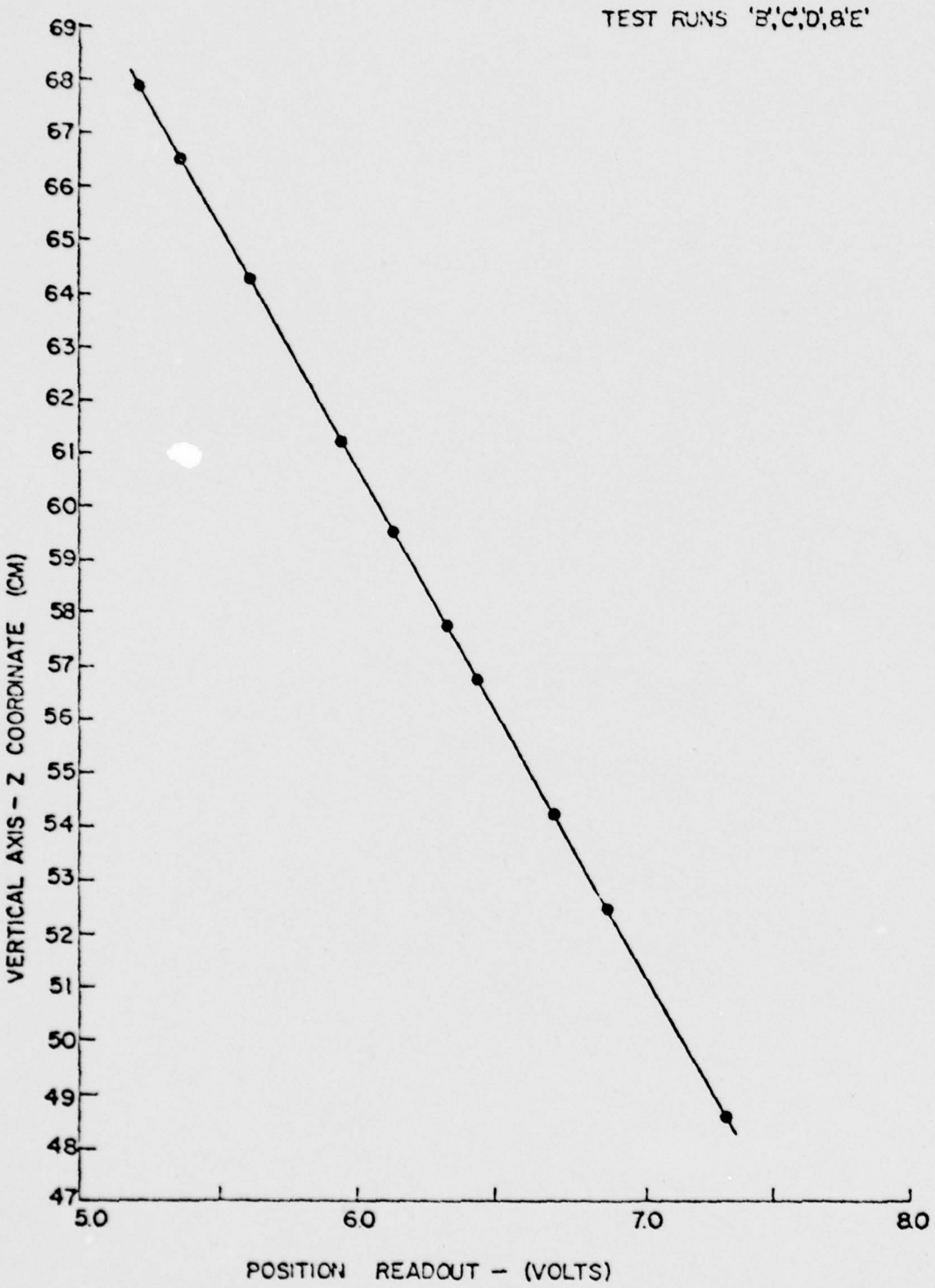


Figure 14. Calibration Curve for Position Indicator Runs B, C, D and E

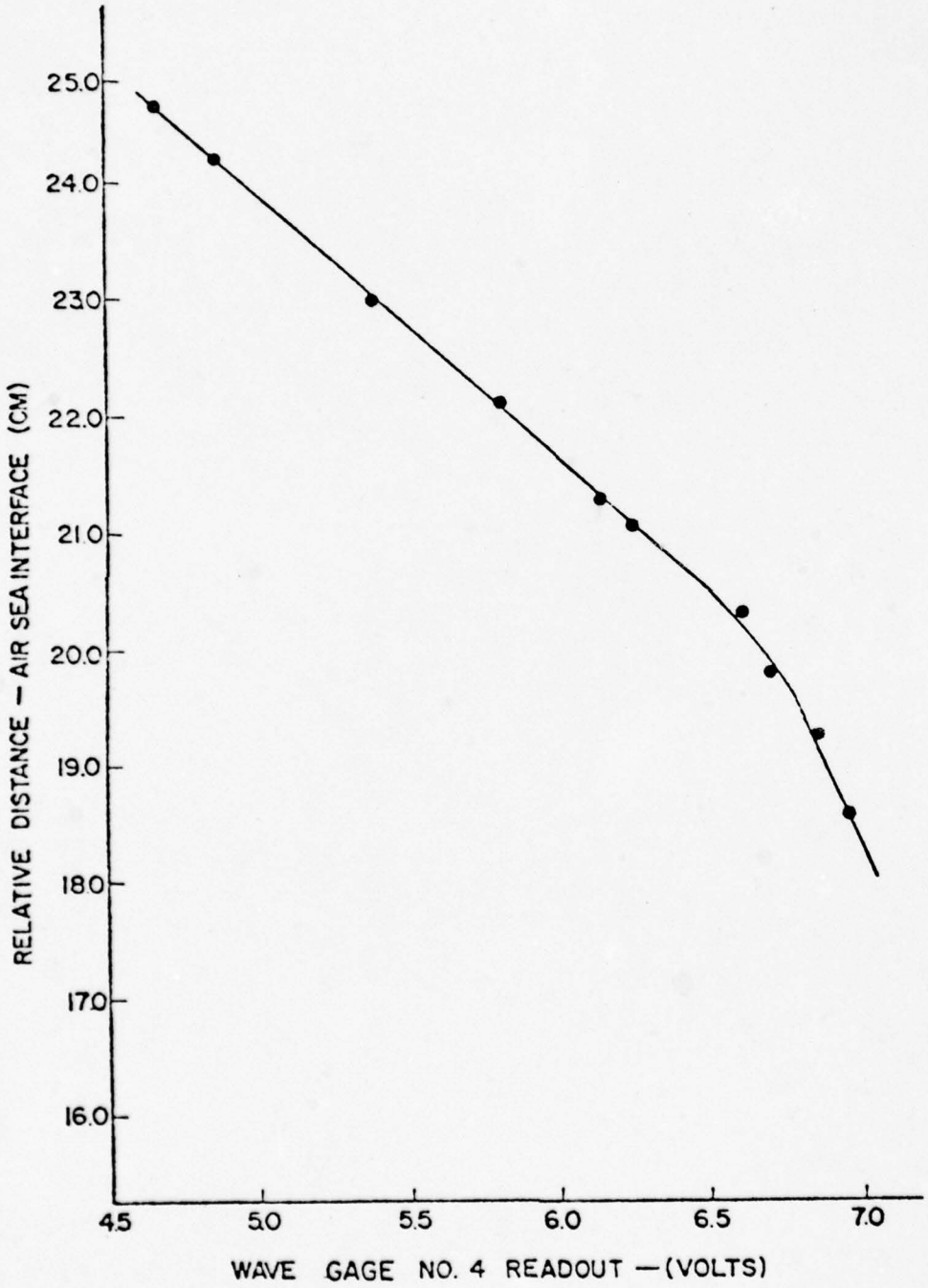


Figure 15. Calibration Curve for Wave Gauge 4

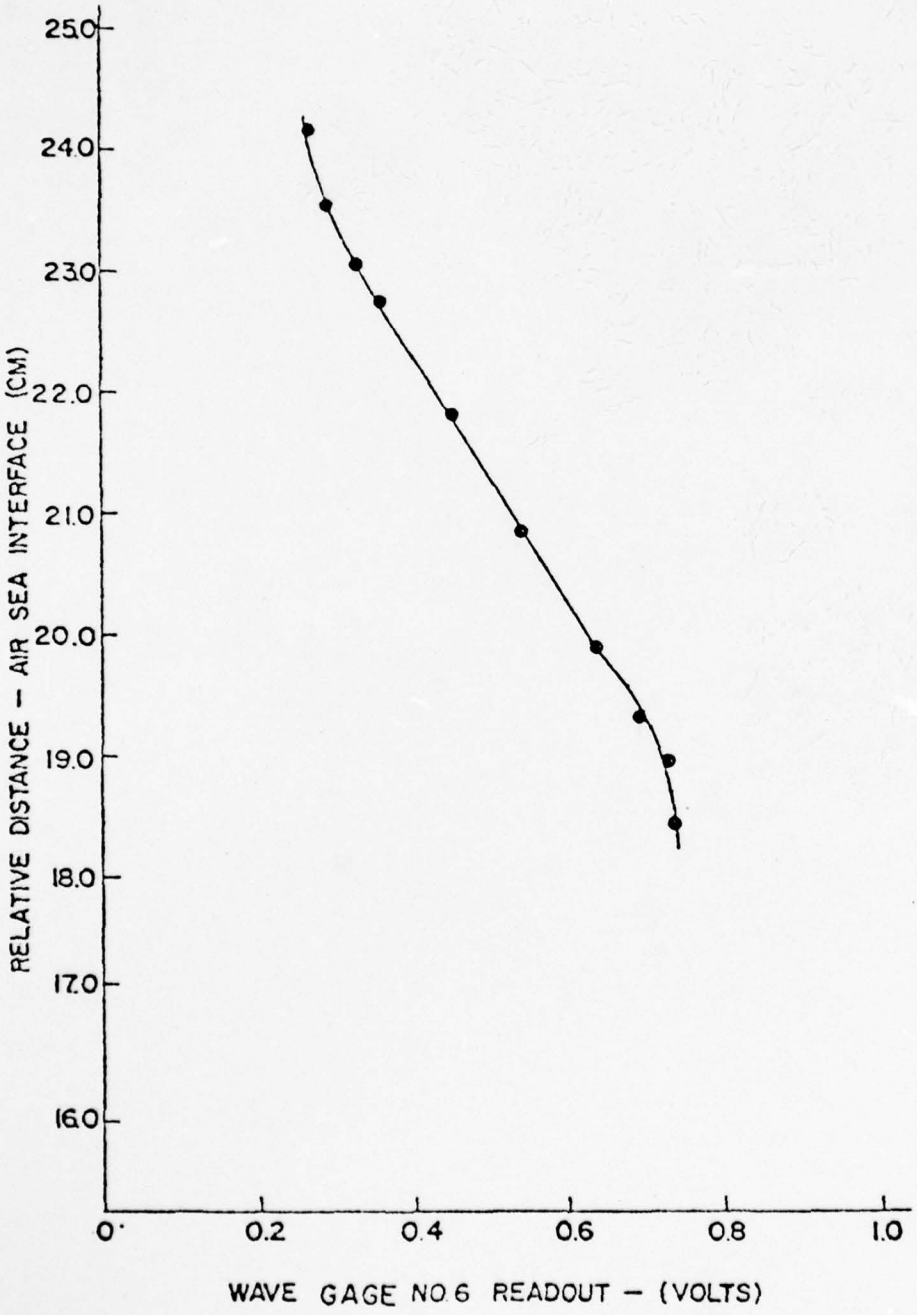


Figure 16. Calibration Curve for Wave Gauge 6

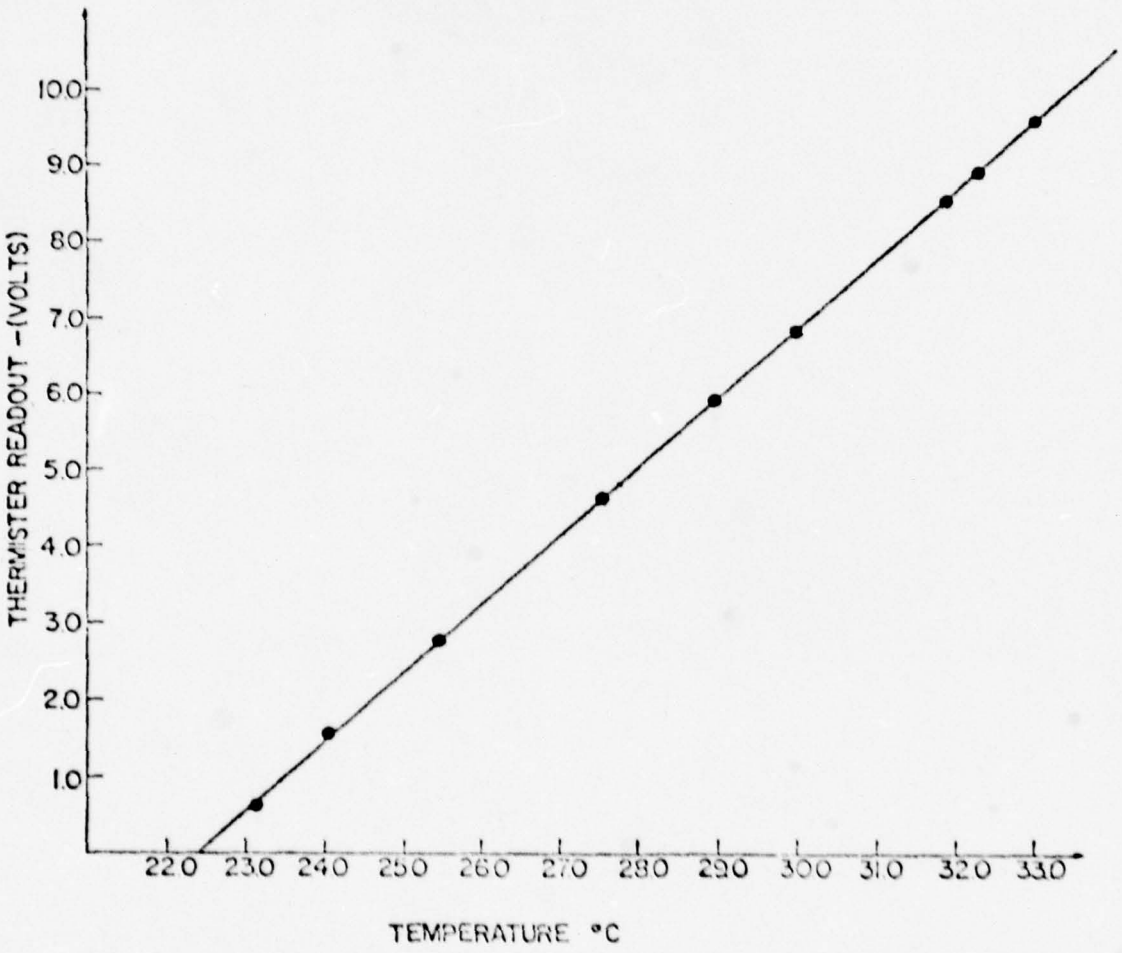


Figure 17. Calibration Curve for Thermistor

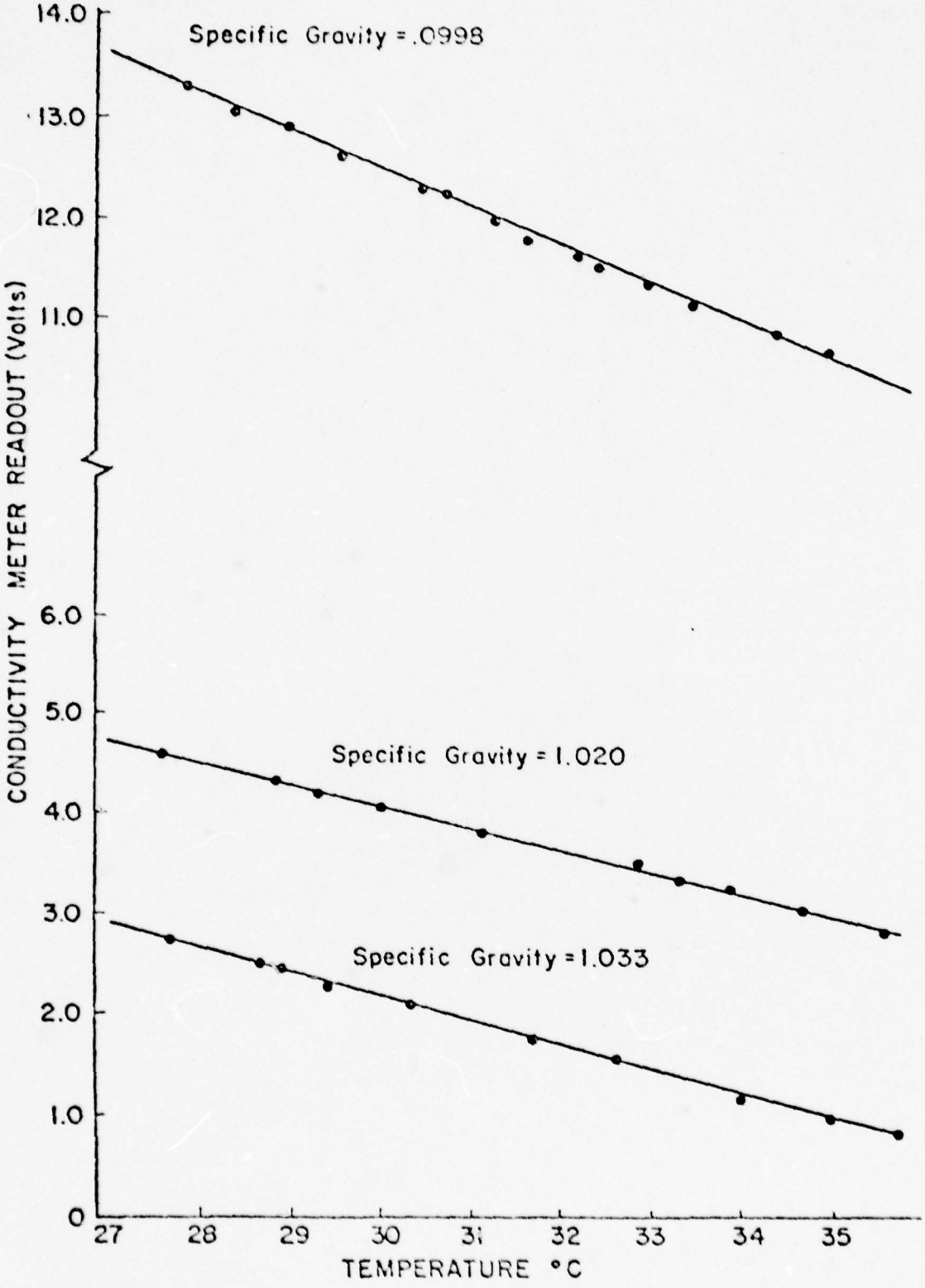


Figure 18. Temperature Effect on Conductivity

CHAPTER VI
MEASUREMENTS

6.1 Test Procedure

The fresh water is gravity fed into the testing tank first then the salt water is slowly gravity fed into the tank through the same inlet at the bottom of the tank. This is done at a slow rate so as to minimize turbulent mixing. As the tank is being filled, the wave gauges are calibrated as described in Section 5.4. Upon completion of the fill procedure, the conductivity probe is calibrated, see Section 5.2. Three full traverses were made for each test run. These traverses ranged from 70cm to 45cm above the tank bottom. The initial or first traverse was made prior to the generation of internal waves. After completing the first traverse, the probes were returned to their upper limit. The wave generator was then energized for a period of time that varied with each test run. The generator was adjusted for the desired frequency and wave amplitude. As the generated waves left the pier the waves were observed to assure that the midpoint of the wave amplitude corresponded to the midpoint of the pier. This was done to assure that the waves do not exceed the top or bottom of the pier. After the waves reached the desired amplitude their approximate amplitude and wave length was noted and recorded. The wave generator was then de-energized, and the motion of the interface allowed to decay to zero. The second full traverse was then made; this information was recorded on magnetic tape and on a chart recorder. Once the traverse was completed the probes were

returned to their upper position. The wave generator was re-energized and the wave amplitude adjusted by observing the chart recorder output. After a period of time, that varied with each test run, the wave generator was de-energized. When the interface stabilized the final traverse was made. Test runs B and D were done on the same evening. Test B diffused the interface so before test run D began the interface was siphoned to sharpen it. Test run D was done in order to gain some insight into the effects of large amplitude internal waves. The a/L ratio for this run was much higher than for runs A, B and C. During the time periods that the interfacial waves were being generated visual observations of the waves and associated phenomena were made and recorded. Photographs of the interface were also taken (see Figure 22). Observations of the formation and growth of waves in the interfacial density layer were made and sketches drawn (see Figure 28). On test run C a shadowgraph was set up in station number 3. A light was projected through the tank and onto a cloth screen on the opposite wall of the tank. Photographs and visual observations of the interface and the density gradient layer were made possible through the use of this shadowgraph (see Figure 22). After completion of data acquisition the salt layer was pumped back into its storage tank and the fresh layer dumped.

6.2 Data Reduction

Signals from the position sensor and the conductivity probe were passed through a preamplifier and low-pass filter circuit (see Figure 29) before being recorded on magnetic tape. The signals were also recorded on a chart recorder. An x-y recorder was then used to plot the tape output. Position was plotted on the y axis and conductivity voltage on the x axis. With the position vs conductivity voltage profiles now

available, point-by-point data reduction was possible by using the appropriate conductivity voltage vs specific gravity calibration curves. With this data reduction completed, the density profiles were then drawn. See Figures 23 through 26. The variations in conductivity voltage as a result of temperature were insignificant; (see Figure 18), therefore, the temperature effects were not taken into consideration in the final density profiles.

Wave frequency, wave length, celerity and wave height were determined as outlined in Section 4.5.

CHAPTER VII
RESULTS, CONCLUSIONS AND RECOMMENDATIONS

The experimental results and visual observations are presented and discussed in this chapter. An interpretation of the results is given along with recommendations for future work.

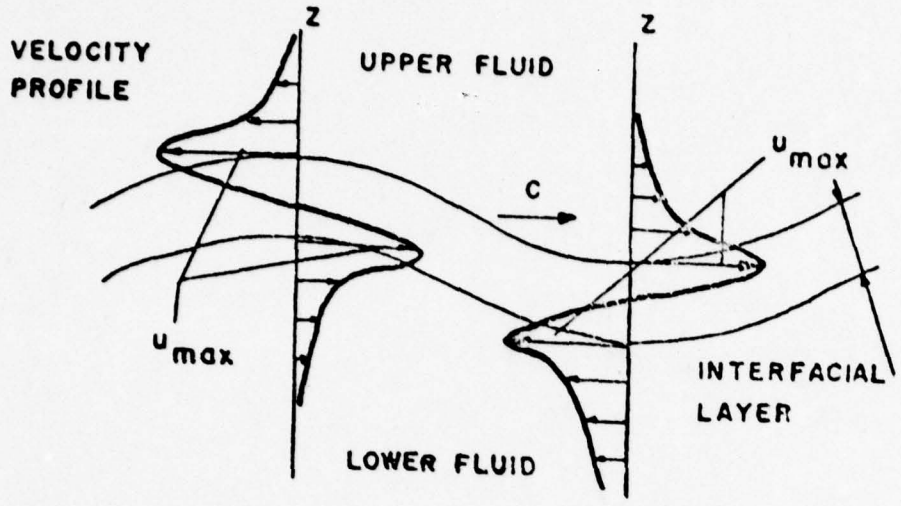
Mixing in a stratified flow can be caused by molecular diffusion and/or turbulence. Mixing caused by molecular diffusion is a relatively slow process when compared to the mixing process caused by turbulence. Molecular diffusion is proportional to the density gradient of the fluid. Turbulence in the flow greatly enhances the mixing process. The initiation of turbulent activity in fluid flow is a complicated process that defies detailed explanation. It can be the result of the growth of infinitesimal disturbances in an unstable flow.

The stability of a stratified shear flow is characterized by the magnitude of the Richardson number

$$Ri = \frac{-\rho' g}{\rho u'^2}$$

as discussed earlier in this thesis.

The propagation of finite amplitude internal waves along the interface of a two layer stratified fluid, creates high shear levels near the interface due to the particle motion generated by the waves. This shear is oscillatory in nature due to the periodicity of the waves and has maximum values at the crests and troughs of the waves. Figure 19 shows a sketch of the instantaneous velocity profiles at the crest and trough of an internal wave at the diffused interface of a two layer stratified fluid system. See Figure 20 for a definition sketch of the flow.



Instantaneous Velocity Profiles in an Internal Wave
at the Diffused Interface of a Two Layer Fluid

Figure 19

In observing the velocity profiles it is noted that the velocity gradient

$$u' = \frac{du}{dz}$$

has a maximum value in the diffused layer (interfacial layer). The magnitude of the maximum velocity gradient is a function of the maximum velocity and the thickness of the interfacial layer. The maximum velocity is proportional to the steepness ratio of the wave. The steepness ratio is the ratio of the wave amplitude to the wave length (a/L). Thus for a given thickness of the interfacial layer the maximum velocity gradient is a

function of the wave steepness ratio. Since the Richardson number is inversely proportional to the square of the velocity gradient, the larger the velocity gradient, the smaller the value of the Richardson number and thus the less stable the flow.

As discussed earlier, a sufficient condition for the stability of an inviscid, incompressible stratified shear flow is that the local or gradient Richardson number be greater than 1/4 throughout the flow. Experimental results Wang (1972) and Scotti (1969) seem to indicate that the critical Richardson number for stratified shear flows in real Newtonian fluids such as air and water is near the 1/4 value.

It was anticipated then, that as the steepness ratio was increased beyond some value, the increasing value of the velocity gradient would result in the value of the Richardson number dropping below the critical value and growth of the ever present infinitesimal disturbances would be observed. An experiment was performed as described in Chapter VI to investigate this instability and to measure the mixing that resulted.

During the experiment the interfacial layer was observed as the mechanically generated internal waves propagated along the interface. The anticipated growth of infinitesimal disturbances was observed. High frequency waves (interfacial waves) grew and appeared within the interfacial layer, as was expected, due to the large velocity gradient within the layer. See Figure 22 for photographs of the interfacial layer and the interfacial waves. It is believed that these interfacial waves resulted from the growth of an infinitesimal disturbance in the unstable interfacial layer.

A schematic representation of the growth and breakdown of the interfacial waves is shown and discussed in Figure 28. The growth and appearance of the interfacial waves would appear and grow, and then break until the

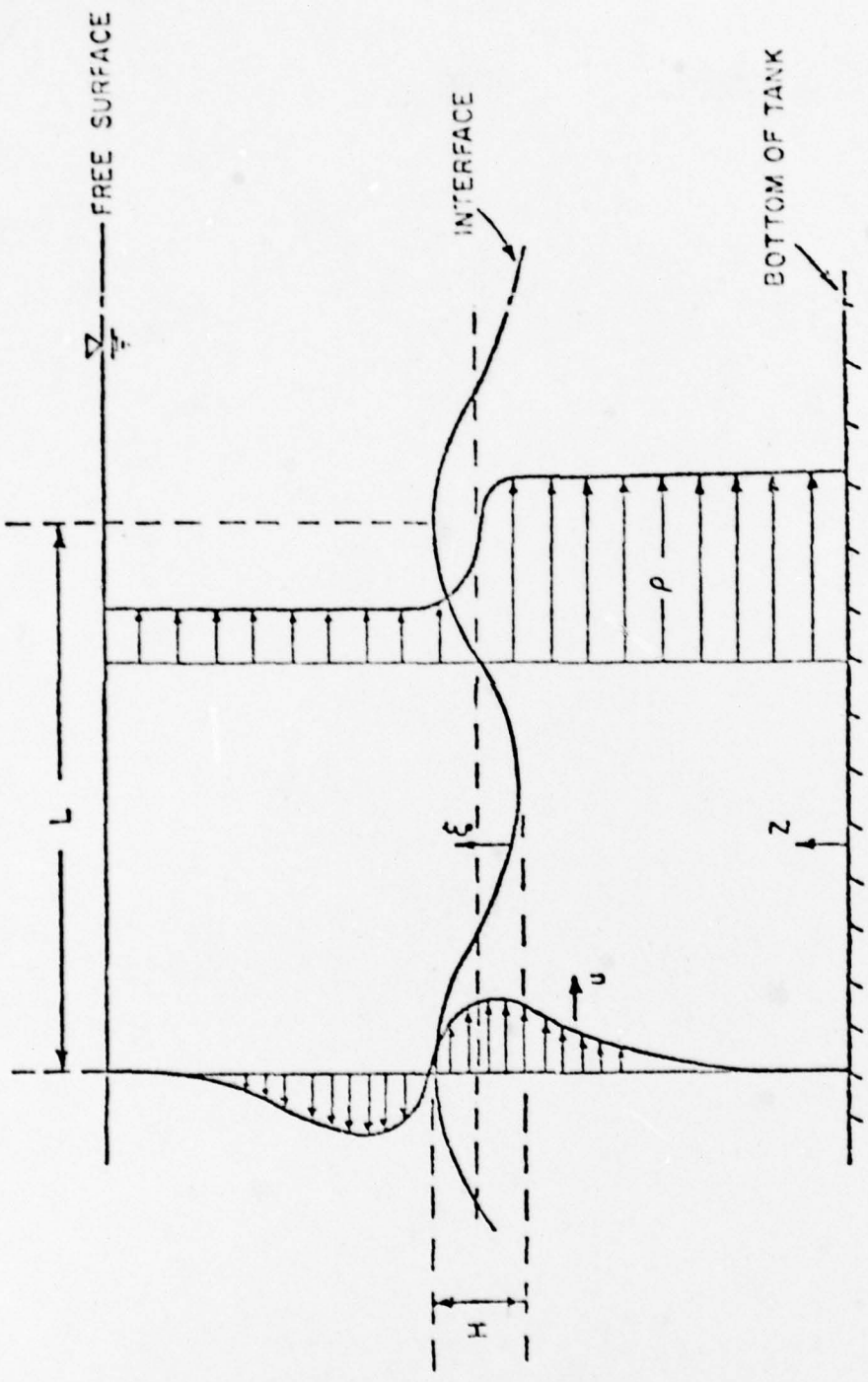


Figure 20. Definition Sketch

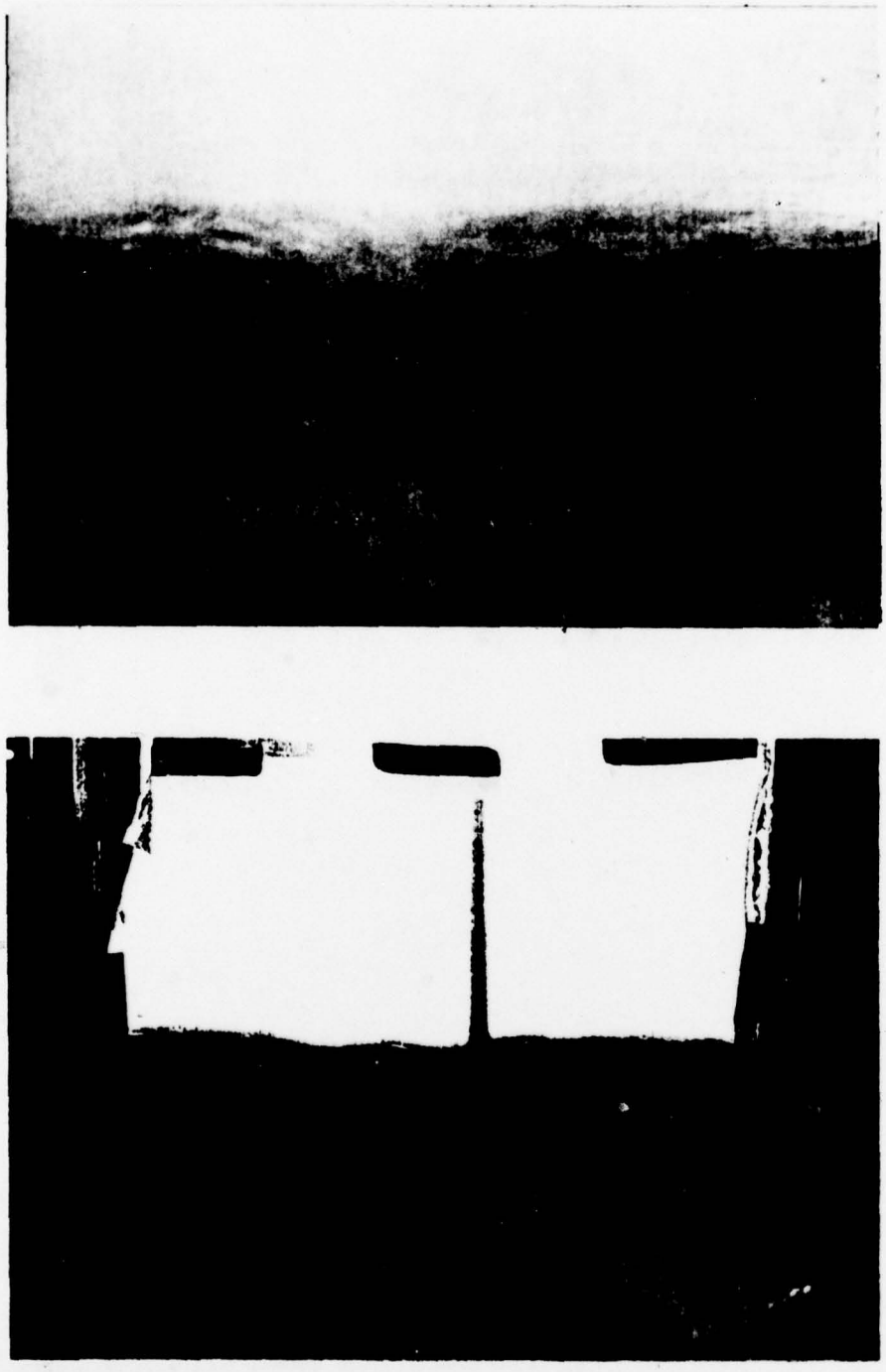


Figure 22. Photographs of Interfacial Layer and Interfacial Waves

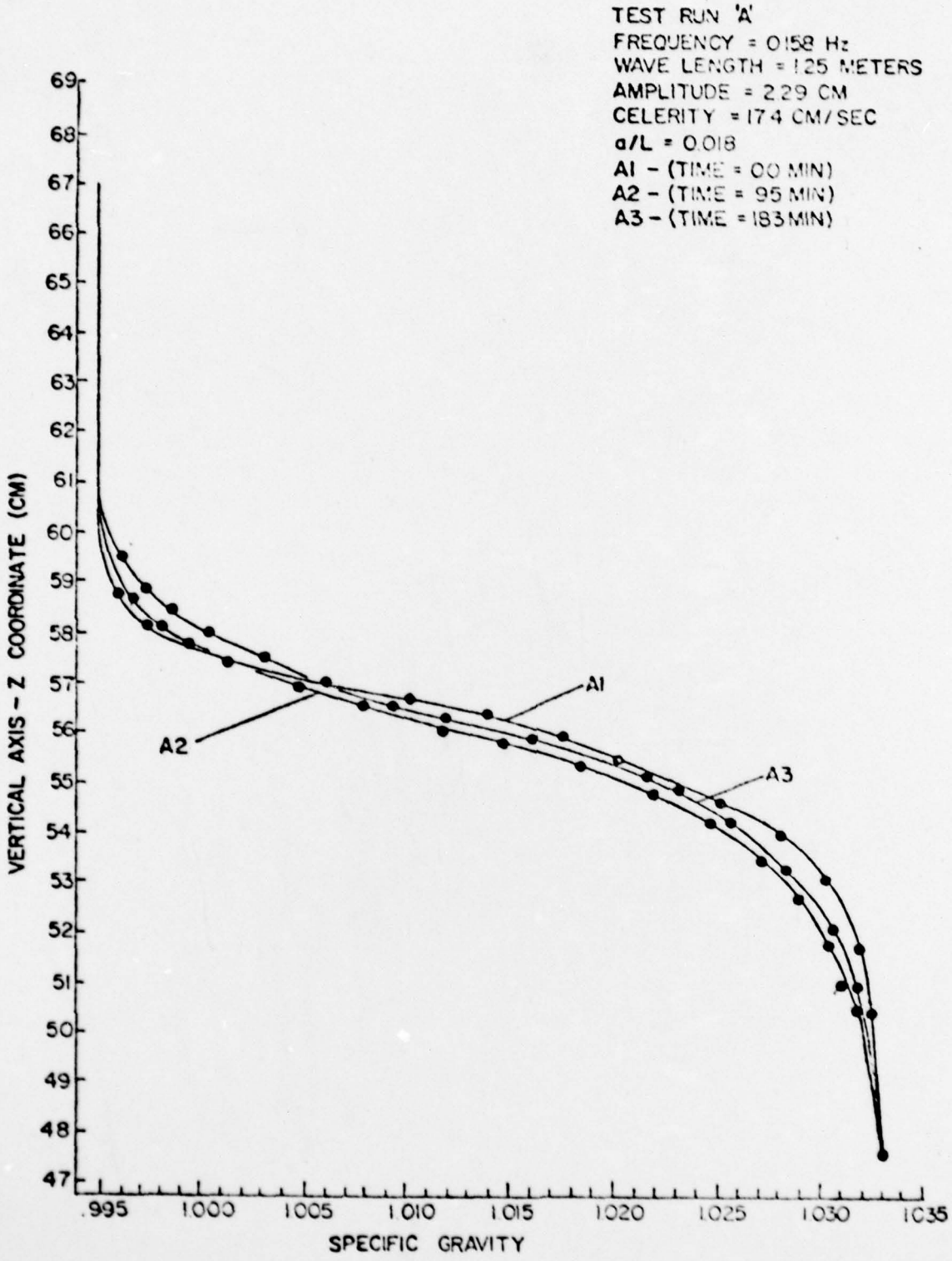


Figure 23. Density Profiles, Run A

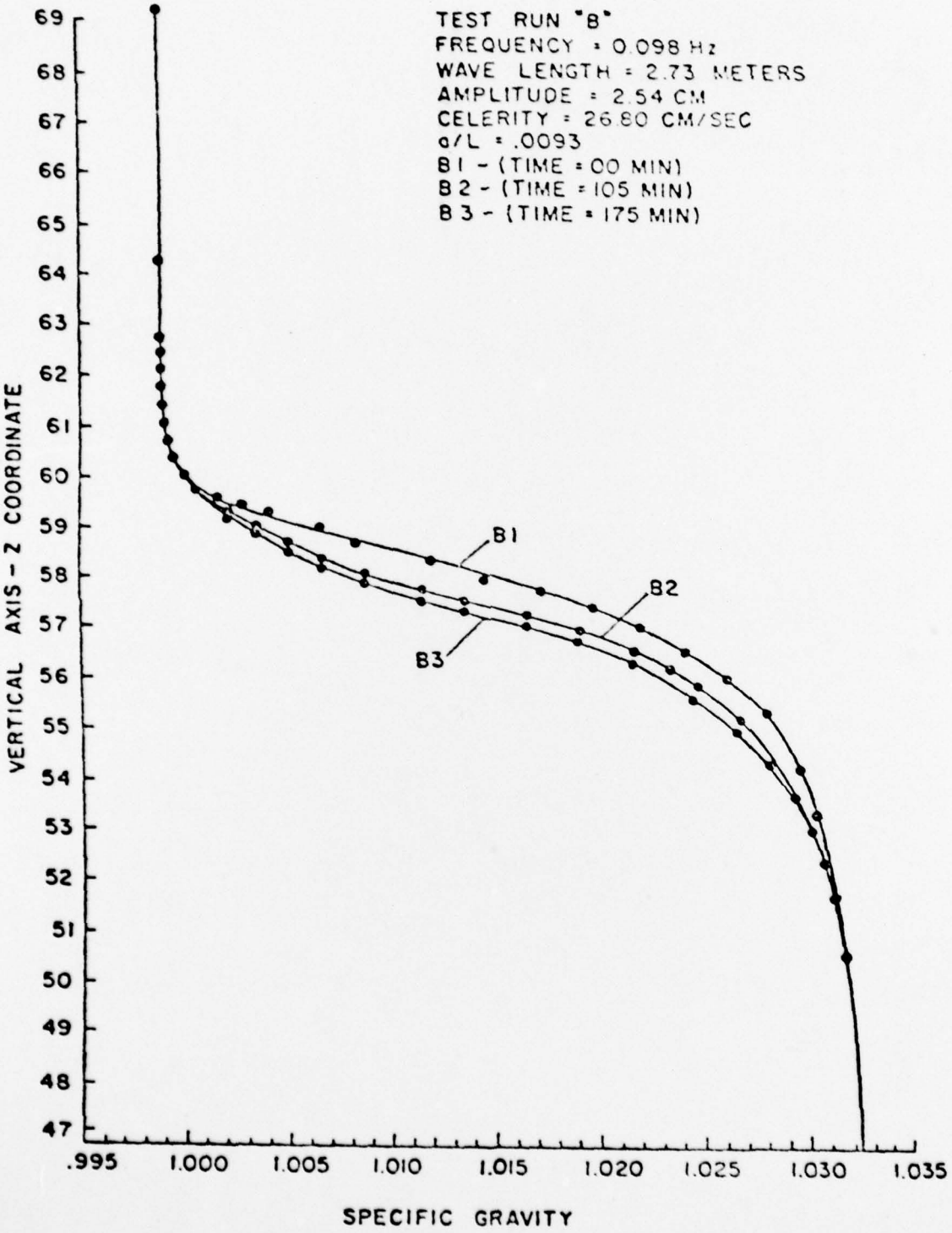


Figure 24. Density Profiles, Run B

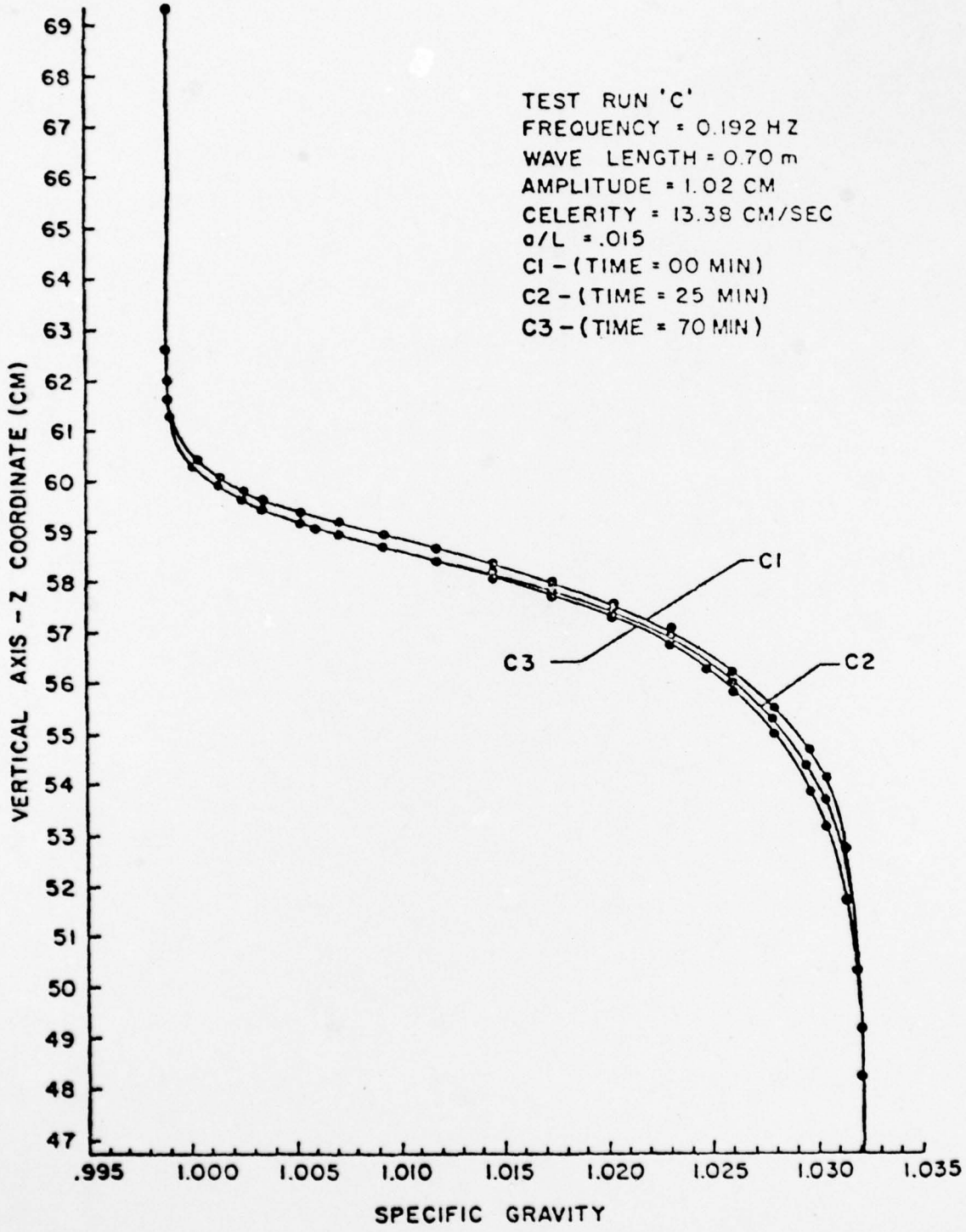


Figure 25. Density Profiles, Run C

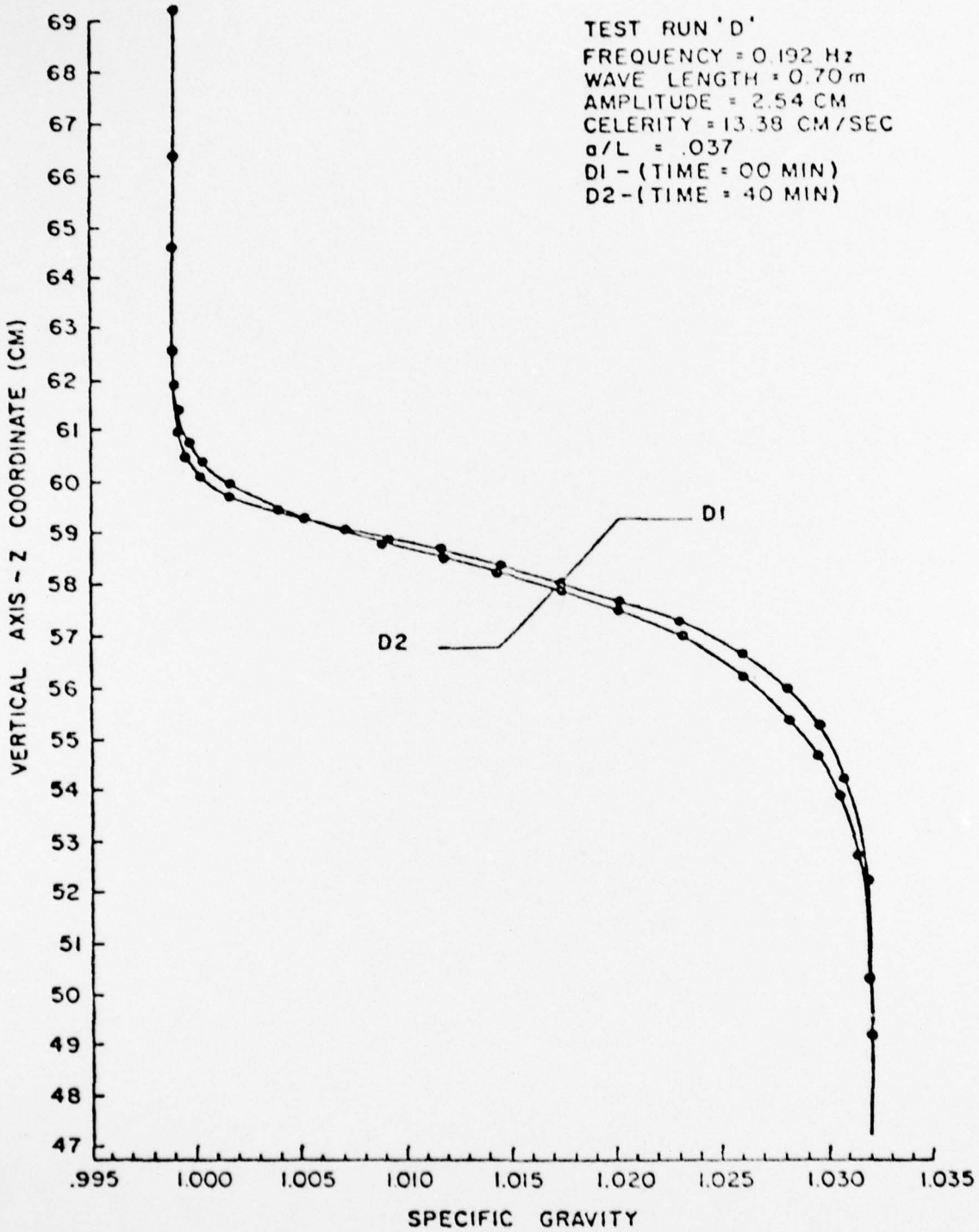


Figure 26. Density Profiles, Run D

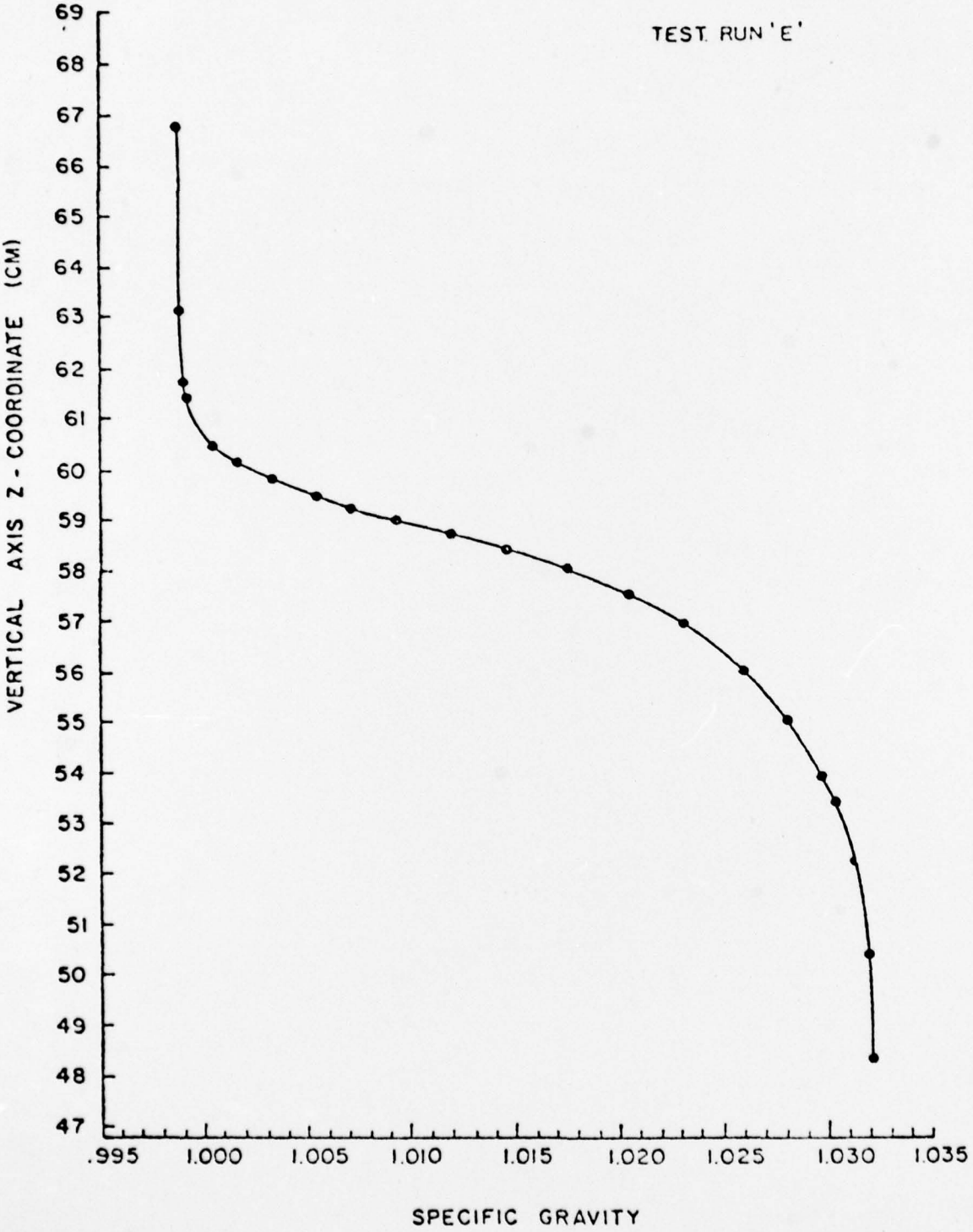


Figure 27. Density Profile, Run E

The actual profiles, however, show only minor changes even over long periods of time. The substantial activity observed within the interfacial layer must have been high frequency internal waves and a form of macro turbulence, lacking the micro turbulent activity that generates mixing. Sufficiently steep internal waves, it is anticipated, could actually generate micro turbulence, but such large waves would mix the fluid to a degree that there would be no discernible interfacial layer.

As the generation of the internal waves was discontinued, the interfacial waves subsided and the interfacial layer appeared to return to its prewave condition of many laminar layers, another indication that very little mixing occurred. In field studies in the European Mediterranian, Woods (1969) observed layers of laminar flow separated by thin "turbulent" layers. These turbulent layers might very well have been layers of high frequency internal waves (interfacial waves) such as those observed in this research.

In examining the data in Figures 23 through 26, some diffusion with time is apparent in all runs except for curves A2 and A3 of test run A (see Figure 23). This apparent anomaly can be explained by the existence of a long wave in the tank, that affected the relative position of the interface during the experiments. To prevent long waves the interface must be allowed to settle completely after filling, and the amplitude of the internal waves must be brought up very slowly as the test run begins. It is noted that the density profiles in Figures 23 through 26 show the most apparent change in the profiles occurred at the knees of the profiles. The profiles vary more noticeably at the knee where the transition from the interfacial layer, to the salt solution layer (red layer) occurred. The slope of the density profile through the interfacial layer changed only slightly with time.

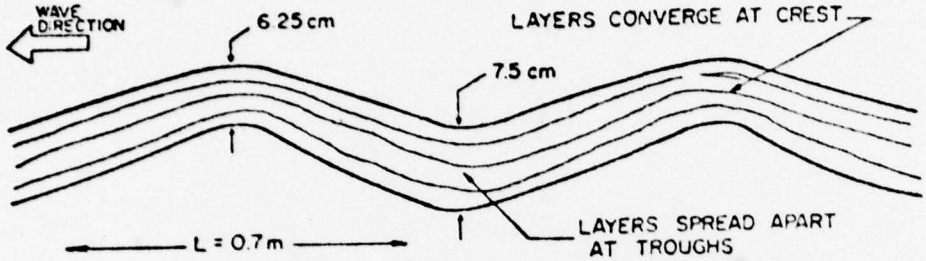
The most significant contribution of this work is the prediction and observation of the higher frequency waves within the interfacial layer. The growth of the high frequency waves in the interfacial layer indicates the layer is unstable. Apparently the instability resulted from the high shear levels created by the internal waves. In these experiments the steepness ratio was sufficiently large for unstable conditions to exist in the interfacial layer. It was anticipated that when interfacial waves existed, substantial mixing would occur, as shown in the profiles in Figure 21. The results of this experiment, however, show the contrary to be true. The lack of substantial mixing as was expected is quite significant.

Some investigators have hypothesized that internal waves might be a primary source of turbulence in the ocean and in the atmosphere. The results of this work by no means rules out this possibility but it does cast some doubt and indicates that further work should be done. This lack of substantial mixing could be good news to some as it relates to certain activities within the ocean. For example in the ocean thermal energy conversion process it is desired that the stratified cool and warmer layers maintain their integrity with as little mixing as possible. The possibility of the generation of internal waves and the resulting turbulent mixing at the interface of the thermally separated fluids due to the discharge of the vast quantities of ocean water used in the thermal conversion system, is a real concern. The results of this work, however, would seem to negate to some extent this concern.

Further investigation of the steepness ratio as it relates to the instability within the interfacial layer is necessary. In these experiments, internal waves of sufficient steepness for unstable flows were

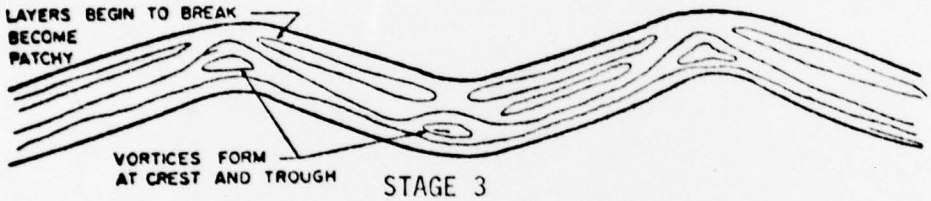
used. Experiments should be conducted to determine the critical value of the steepness ratio that would insure the growth of the infinitesimal disturbances present within the fluid system. In this experiment, velocity measurements were not made due to the continuing failure of the hot film probe. Velocity profiles were needed so that plots of the Richardson number profiles could be made. With this information available, the critical steepness ratio value could be compared with the experimentally determined Richardson number profile and then both of these values can be compared to the theoretically determined critical Richardson number. In this experiment the dominant frequency of the interfacial waves was not determined. Further experiments are required to determine this frequency and how it relates to the frequency of the primary internal wave. The frequency of the interfacial wave could also be compared to the value of the natural frequency (Brunt-Väisälä) for the interfacial layers. The most interesting aspect of the experiment is the relatively small amount of mixing that occurred even in the interfacial layer where at times it visually appeared to be turbulent. It is suggested that future experiments include sufficiently large values of steepness ratio so that substantial mixing will occur. By working up to these large values of steepness ratios, the transition point from macro to micro turbulence could be investigated.



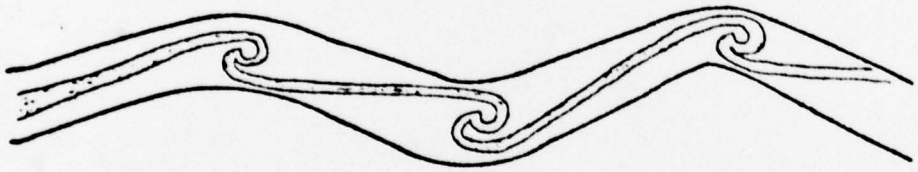


LAMINAR LAYER SET INTO WAVE FORM MOTION BY GENERATION OF INTERNAL WAVES

STAGE 2

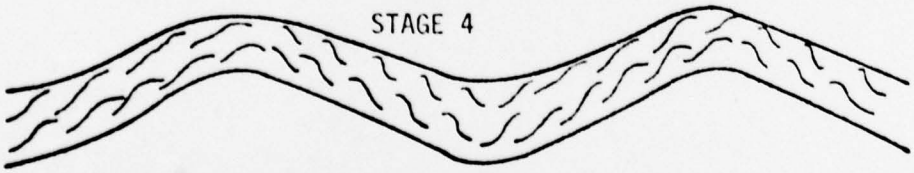


STAGE 3



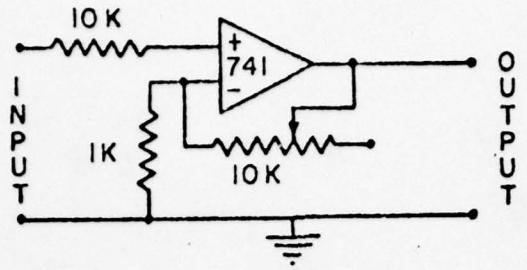
LAYERS BEGIN TO ROLL AND OVERTURN AT VORTEXES AS REGION WITH LAYER BECOMES UNSTABLE RESULTING IN TURBULENT MIXING

STAGE 4

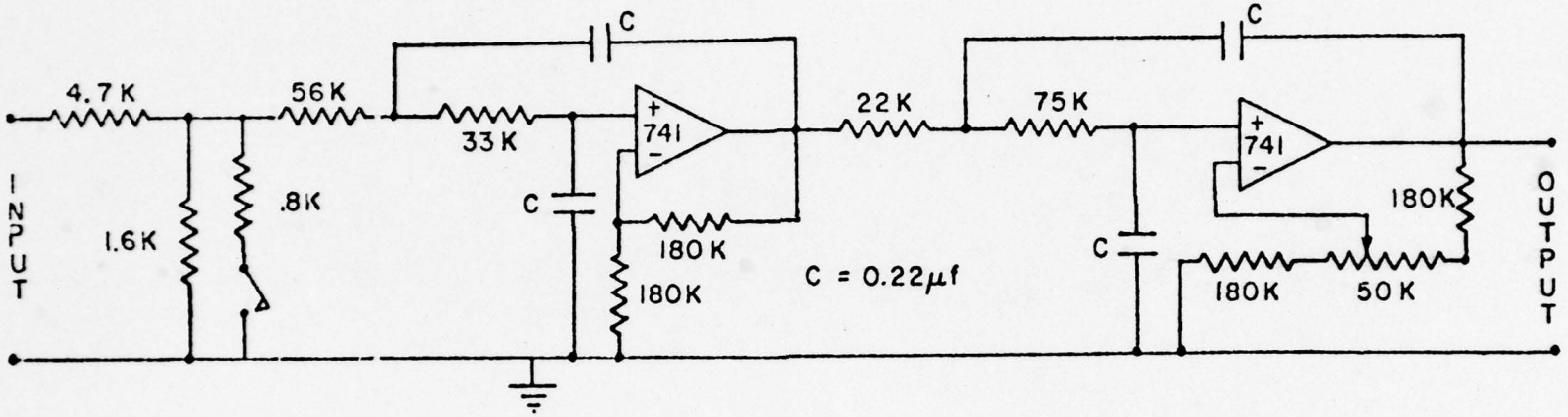


INTERFACIAL WAVES SHOWN WITHIN INTERFACIAL LAYER

Figure 28. Schematic Formation of Interfacial Waves



PRE-AMP CIRCUIT



LOW-PASS FILTER CIRCUIT

Figure 29. Pre-amplifier and Low-pass Filter Circuit

BIBLIOGRAPHY

Doddington, H.W. and D.M. Sheppard, (1974), "A Laboratory Instrument for Measuring Electrical Conductivity in Stratified NaCl Solution," Submitted to the Editorial Office of the Review of Scientific Instruments.

Hall, J.M. and Yih-Ho Pao, (1969), "Spectra of Internal Waves and Turbulence in Stratified Fluids," Radio Science, Vol. 4, Number 12 pp. 1321-1325.

Hazel, P., (1972), "Numerical Studies of the Stability of Inviscid Shear Flows," J. Fluid Mech., Vol. 51, part 1, pp. 39-61.

Long, R.R., (1965), "On the Boussinesq Approximation and its Role in the Theory of Internal Waves," Tellus XVII, pp. 46-52.

Long, R.R., (1973), "Some Properties of Horizontally Homogeneous, Statistically Steady Turbulence in a Stratified Fluid," Boundary-Layer Meteorology 5, pp. 139-157.

Pao, Yih-Ho, (1969), "Spectra of Internal Waves and Turbulence in Stratified Fluids," Radio Science, Vol. 4, Number 12, pp. 1315-1320.

Powell, G.M. and D.M. Sheppard, (1974), "A Laboratory Optical Internal Wave Gage," College of Engineering, University of Florida, July, 1974.

Scotti, R.S. and G.M. Corcos, (1969), "Measurements on the Growth of Small Disturbances in a Stratified Shear Layer," Radio Science, Vol. 4, Number 12, pp. 1309-1313.

Scotti, R.S. and G.M. Corcos, (1971), "An Experiment on the Stability of Small Disturbances in a Stratified Free Shear Layer," J. Fluid Mech., Vol. 52, part 3, pp. 499-528.

Sheppard, D.M., O.H. Shemdin and Y.H. Wang, (1973), "A Multipurpose Internal Wave Facility," Department of Coastal and Oceanographic Engineering, Technical Report No. 19, University of Florida, June, 1973.

Thorpe, S.A., (1968), "A Method of Producing a Shear Flow in a Stratified Fluid," J. Fluid Mech., Vol. 32, part 4, pp. 693-704.

Turner, J.S., (1973), Buoyancy Effects in Fluids, Cambridge University Press.

Wang, Y.H., (1972), "An Experimental Study of a Discontinuously Stratified Shear Layer," Ph.D. Dissertation, University of Southern California.

Woods, J.D., (1968), "Wave-Induced Shear Instability in the Summer Thermodine," J. Fluid Mech., Vol. 32, part 4, pp. 791-800.

Woods, J.D., (1969), "On Richardson's Number as a Criterion for Laminar-Turbulent-Laminar Transition in the Ocean and Atmosphere," Radio Science, Vol. 4, Number 12, pp. 1289-1298.

Yih, Chia-Shun, (1965), Dynamics of Nonhomogeneous Fluids, Macmillan.